Remote Sensing of Environment 139 (2013) 81–96

Contents lists available at ScienceDirect

Remote Sensing of Environment

journal homepage: www.elsevier.com/locate/rse

Microwave emissivity of sea foam layers with vertically inhomogeneous dielectric properties

Magdalena D. Anguelova *, Peter W. Gaiser

Naval Research Laboratory, Remote Sensing Division, Washington, DC 20375, United States

ARTICLE INFO

Article history:
Received 24 August 2012
Received in revised form 9 July 2013
Accepted 19 July 2013
Available online 28 August 2013

Keywords:
Sea foam emissivity
Microwave emissivity
Passive remote sensing
Emissivity model
Foam-covered sea surface
Foam fraction
Whitecap fraction
Sea foam layers

ABSTRACT

We present a radiative transfer model for the emissivity of vertically structured layers of sea foam at microwave frequencies from 1 GHz to 37 GHz. The main features of the model are: (1) Continuous variation in the amount of air in the foam layer depth which affects foam emission through vertically inhomogeneous foam properties. (2) Various radiative terms contributing to foam emissivity, such as upwelling and downwelling emissions within the foam layer, emission of seawater beneath the foam, and multiple reflections of these components at the foam layer interfaces. (3) Distribution of foam layer thicknesses. The dependencies of foam emissivity on foam layer thickness and incidence angle are presented. Analysis of the model sensitivity to input parameters shows that its results are most affected by the choice of the void fraction value at the air–foam interface. Comparisons of the model results to published experimental and modeling data show that with fewer model variables and inputs, and with a single tuning parameter, the model performs as well as, or better than, other physical models.

Published by Elsevier Inc.

1. Introduction

Interest in studies of sea foam (whitecaps) in the ocean has increased recently for two reasons. First, sea foam has a strong signature in various portions of the electromagnetic (EM) spectrum (Koepke, 1986) and with this the potential to influence the accuracy of geophysical retrievals and climate predictions employing these retrievals. Including foam effects in forward models of retrieval algorithms is one possible way to meet the demand for high accuracy in retrieving wind vector (Bettenhausen et al., 2006) and salinity (Zine et al., 2008) from passive microwave measurements. A necessary element of implementing this is a model of the emissivity of a sea surface 100% covered with sea foam e_f. This need has motivated the collection of new experimental data (Camps et al., 2005; Padmanabhan, Reising, Asher, Rose, & Gaiser, 2006; Rose et al., 2002) and the development of emissivity models (Chen et al., 2003; Guo, Tsang, Asher, Ding, & Chen, 2001; Raizer, 2007; Reul & Chapron, 2003) useful to understand and characterize the remote sensing signature of sea foam at microwave frequencies.

Second, sea foam is involved in a long list of climate relevant processes, including sea spray aerosol production (Blanchard, 1963; de Leeuw et al., 2011; Lewis & Schwartz, 2004; Monahan, Fairall, Davidson, & Boyle, 1983), heat exchange and intensification of tropical cyclones (Andreas, 2010; Andreas, Persson, & Hare, 2008), gas exchange (Wanninkhof, Asher, Ho, Sweeney, & McGillis, 2009), and ocean surface albedo (Kokhanovsky, 2004). These processes are, or can be, incorporated in climate models via whitecap fraction W. To adequately model air–sea interaction processes important for the climate system, improvement of both measurements of W and quantification of the spatial and temporal variability of W are pursued (de Leeuw et al., 2011). Part of these efforts is to estimate W on a global scale from routine satellite-based microwave measurements (Anguelova, Bettenhausen, & Gaiser, 2006). Anguelova and Webster (2006) demonstrated the feasibility of global radiometric measurements of W and suggested several improvements in its initial implementation, including a more comprehensive model of foam emissivity e_f.

The development of a foam emissivity model requires knowledge of foam characteristics and properties in order to make valid assumptions and, if needed, simplifications. Faced with incomplete knowledge of sea foam interaction with EM radiation at microwave frequencies, we explored foam dielectric and radiative properties in a series of papers. We started with an investigation of the complex permittivity of sea foam ε_f (Anguelova, 2008). Specifically, we analyzed available information on a plethora of existing formulae (mixing rules) to determine the most suitable one for computing ε_f; considered the dependences of ε_f on both seawater temperature and salinity; and assessed variations in sea foam emissivity e_f based on the choice of a mixing rule for ε_f. We continued with an examination of the skin depth of foam layers

* Corresponding author at: Remote Sensing Division, Code 7223, Naval Research Laboratory, 4555 Overlook Ave. S.W., Washington, DC 20375-5320, United States. Tel.: +1 202 404 6342; fax: +1 202 767 7885.
E-mail address: maggie.anguelova@nrl.navy.mil (M.D. Anguelova).

0034-4257/$ – see front matter. Published by Elsevier Inc.
http://dx.doi.org/10.1016/j.rse.2013.07.017

with a vertical void fraction profile (Anguelova & Gaiser, 2011, hereinafter AG11). In this study, we also studied various functional forms to model foam void fraction. From analysis of foam skin depth and the possible reasons for its variation, we gained insights on the frequency sensitivity to foam thickness, deduced emissivity regimes of foam layers, each associated with specific e_f variations depending on the foam layer thickness, and used these results to infer useful implications for remote sensing of whitecaps. We finished this series of investigations with an analysis of intrinsic foam parameters such as foam impedance, size parameter, and refractive index (Anguelova & Gaiser, 2012, hereinafter AG12). This last study helped us to identify unique properties of the fundamental radiative processes of reflection, scattering, and transmission through vertically structured foam layers. The main result was the formulation of a general concept of how the vertical inhomogeneity of dielectric properties leads to the high, blackbody-like emissivity of sea foam.

The findings, insights, and generalizations in this series of papers form the physical basis of the work presented in the current paper. Here we report results of a radiative transfer (RT) model of the emissivity e_f of vertically structured layers of sea foam at microwave frequencies from 1 GHz to 37 GHz. A summary of the physical and dielectric properties of sea foam (Section 2.1) helps to formulate requirements for modeling e_f (Section 2.2). A review of previous models of foam emissivity, both empirical (Sections 2.3) and physical (Section 2.4), helps to determine which approach and model parameters could meet these requirements. After justifying some assumptions and simplifications (Section 3.1), we describe the elements of our model (Sections 3.2–3.4) and present its results (Section 4). We then proceed to analyze the model's sensitivity to choices of input values (Section 5.1), compare the model results to experimental data and those of other models (Section 5.2), and evaluate the model performance (Section 5.3). We finish with a summary of the major features and results of the foam emissivity model (Section 6).

2. Modeling microwave foam emissivity

While sea foam can be defined broadly to include bubble plumes in seawater, foam layers at the surface, and, in some cases, sea spray droplets suspended closely above the surface (e.g., Newell & Zakharov, 1992), the foam skin depth at microwave frequencies narrows the scope to the surface expression of sea foam (AG11). We model, therefore, the emissivity of a foam layer floating on the surface and the dense bubbly mixture immediately below. Deeper bubble plumes and sea spray flying over foam-free or foam-covered areas also affect microwave signals (Barber & Wu, 1997; Plant, 2003; Tang, 1974). However, we do not consider their effects for now. Adopting the most widely used oceanographic terminology to distinguish active (newly-formed) and residual (decaying) sea foam, we state our interest in both of these stages of whitecaps [refer to Anguelova (2008, Section 2.1) for an extended foam definition]. Although modeling the emissivity of these two stages separately can be useful for air–sea interaction and remote sensing studies (AG11, Section 4.3; Anguelova & Hwang, 2012), we do not attempt such a separation in this study.

2.1. Overview of sea foam properties

A layer of sea foam floating on the surface is an air–water mixture, with the seawater being an environment in which air bubbles are inclusions. To characterize sea foam and the processes within, the bubble dimensions (radius r and wall thickness w) and concentration or size distribution $N(r)$ are necessary. In addition to these microscopic characteristics, a set of macroscopic characteristics, including foam layer thickness t and foam void fraction f_a (defined as the fraction of a unit volume of ocean occupied by air), describes the foam layer as a whole. These micro or macro characteristics establish a group of "medium" variables that represent the specific mechanical structure of sea foam.

A second group of "sensor" variables is needed to describe the detection of foam by sensors operating at various frequencies F and polarizations P (P = H or V for horizontal or vertical polarization, respectively) at various incidence angles θ (Padmanabhan et al., 2006; Rose et al., 2002; Smith, 1988).

The mechanical structure of a layer of sea foam on the ocean surface comprises densely packed bubbles whose dimensions gradually change within the layer thickness (Anguelova, 2008). Large, thin-walled bubbles in the upper part of the foam layer provide low seawater content $Q = 1 - f_a$ and thus form dry foam. As the bubbles become smaller and thicker-walled with depth, the air content f_a decreases, making the foam wet. As a result of this vertical stratification of foam mechanical structure and foam constituent contents, both micro and macroscopic foam characteristics acquire a wide range of values. For example, void fraction could cover a full range of possible values, from approximately 100% at the air–foam interface to less than 1% at the foam–water interface (Anguelova, 2008, Section 2.2). The vertical stratification of the mechanical structure [e.g., $w(z)$] and constituents [e.g., $f_a(z)$] of the sea foam leads to a vertical profile of the foam complex dielectric constant (relative permittivity, hereafter "relative" is omitted) $\varepsilon_f(z)$ (Anguelova, 2008). This, in turn, dictates changes in all other dielectric properties of the sea foam (AG11; AG12).

Because of the dependence of seawater permittivity on seawater temperature T_s (Klein & Swift, 1977; Meissner & Wentz, 2002; Stogryn, 1997), variations of T_s within the foam mixture may result in variations of foam temperature in the foam layer depth $T_f(z)$. Whether foam structure and constituents are constant (i.e., w = const, f_a = const) or varying [i.e., $w(z)$, $f_a(z)$] with depth, the foam temperature profile $T_f(z)$ would create the possibility for vertical inhomogeneity of foam dielectric properties $\varepsilon_f(z)$.

Laboratory and field measurements have shown that sea foam has high, blackbody-like emissivity at microwave frequencies (Nordberg, Conaway, Ross, & Wilheit, 1971; Rose et al., 2002; Smith, 1988; Williams, 1971). According to Kirchoff's law of thermal radiation (Peake, 1959), this suggests that foam is a highly absorptive medium. The close packing of bubbles within a layer of floating foam suggests possible further attenuation due to volume scattering that occurs when $\partial\varepsilon_f(z)/\partial z \neq 0$. Since absorption, scattering, and transmission of EM radiation through a medium are determined by its dielectric properties, $\varepsilon_f(z)$ varying with depth leads to variations in depth of the radiative losses due to absorption and scattering.

If volume scattering is present in a medium with a dielectric profile $\varepsilon_f(z)$, multiple reflections within the medium should be treated as incoherent processes (Ulaby, Moore, & Fung, 1981, Section 4–14). That is, for each reflection among many scatterers only changes in the amplitude of the radiation field need to be accounted for because changes in the phase of the propagating radiation are randomly distributed.

Available photographs show that air–foam and foam–water boundaries are easily discernible, clearly distinguishing the foam layer as a separate entity from the bubble plume below (Peltzer & Griffin, 1987, Fig. 6b; Camps et al., 2005, Fig. 5). If the media on both sides of these boundaries are sufficiently dissimilar dielectrically, the boundaries will cause multiple reflections and transmissions of the radiation propagating through or emitted by the foam. Moreover, if these boundaries are rough on scales smaller than the wavelength of the propagating microwave radiation, these multiple reflections will deviate from specular reflection, giving rise to scattering from the rough surface.

Foam layer thicknesses encountered in the open ocean can range, depending on the wind speed, from 1 cm to more than 20 cm in active whitecaps and from at least 0.1 cm to 1 cm in residual foam (AG11, Section 2.5). Since various meteorological and oceanographic conditions affect the formation of new foam patches and their evolution from young to mature foam, there is a distribution of foam thicknesses throughout the process (Reul & Chapron, 2003).

2.2. Requirements for foam emissivity model

The overview of sea foam properties in Section 2.1 provides a guide to formulating general requirements that a model for the microwave foam emissivity must meet. These are:

1) Model in terms of medium variables represented either with microscopic [r, w, and $N(r)$] or macroscopic (f_a and t) quantities;
2) Model suitable for a range of sensor variables (F, P, and θ);
3) Vertical stratification of the foam structure expressed as vertical profiles of either microscopic [e.g., $w(z)$] or macroscopic [e.g., $f_a(z)$] characteristics;
4) Vertically inhomogeneous foam thermodynamic temperature $T_f(z)$;
5) Non-uniform profile of foam dielectric properties in depth $\varepsilon_f(z)$ due to either vertical variations of $f_a(z)$ [or $w(z)$] or $T_f(z)$ or both.
6) Loss in foam due to absorption and incoherent volume scattering;
7) Surface scattering at irregular air–foam and foam–water boundaries;
8) Multiple reflections and transmissions at the boundaries of the foam layer;
9) A distribution of foam structural characteristics such as bubble dimensions (in microscopic terms) or foam layer thicknesses (in macroscopic terms) in open ocean due to geographic, meteorological and oceanographic variability.

Knowing what needs to be modeled, we review previous modeling efforts. Both empirical and physical models for microwave foam emissivity have been published.

2.3. Empirical models of foam emissivity

Stogryn (1972) used reported radiometric measurements of foam to propose a model for the microwave emissivity of a 100% foam-covered sea surface. The model involves the product of two functions — one introducing a dependence only on incidence angle θ (from 0 to 70°), and another presenting a dependence only on radiation frequency F (from 13.4 to 37 GHz).

Wilheit (1979) does not model foam emissivity specifically, but accounts for the effect that foam has on the surface reflectivity by evaluating how much foam reduces it. The expression contains dependence on F and wind speed U.

Wentz and Meissner (2000) and Bettenhausen et al. (2006) follow an approach similar to Wilheit and model the modification of the surface reflectivity caused by foam. This is done either by multiplying the surface reflectivity by or adding to it an empirical factor (determined from collocated satellite and buoy observations), which is a function of U and sea surface temperature (SST).

A common aspect of empirical models of the foam emissivity, or its effect on sea surface reflectivity, is that they do not involve the physical characteristics of foam as a medium, but instead only take into account dependence on sensor parameters, θ and F, or environmental variables, such as U and SST.

2.4. Physical models of foam emissivity

Physics-based models of microwave foam emissivity extend classical electromagnetic and microwave remote sensing theories of emissivity and volume scattering of a medium with both uniform and non-uniform profiles of physical properties (Brekhovskikh, 1980; Landau & Lifshitz, 1960; Sharkov, 2003, Chapter 7; Tsang, Kong, & Shin, 1985; Ulaby et al., 1981). Applied specifically to foam (in their entirety or just elements of them), these theories have a variety of ways to take into account the physical properties of foam.

The first physical model of foam emissivity e_f was that proposed by Droppleman (1970). The model uses the effective dielectric constant of porous material [Anguelova (2008) established that this is in fact the well-known Maxwell–Garnett mixing rule] and a constant void fraction of foam. Droppleman investigated the dependence of e_f on the foam layer thickness and void fraction at four frequencies ranging from 1.4 GHz to 34 GHz. He used the so-called coherent approach (Ulaby, Moore, & Fung, 1986, Chapter 18), which results in emissivity being an oscillating function of foam layer thickness at a fixed void fraction and frequency.

Like Droppleman (1970), most reported models of foam emissivity do not address the vertical non-uniformity of foam (Camps et al., 2005; Chen et al., 2003; Dombrovskiy, 1979; Dombrovskiy & Raizer, 1992; Guo et al., 2001; Zhang, Yang, & Kong, 2002; Zhou, Tsang, & Chen, 2003). These models use constant foam temperature and an effective dielectric constant representative of one specific void fraction of the foam (usually a value from 90% to 95%), which is chosen either directly or through the choice of bubble dimensions.

2.4.1. Modeling the vertical structure of sea foam

For any dielectric medium in general, the problem of non-uniform vertical profile has been systematically investigated since the late 1960s (Sharkov, 2003, Section 7.7). Stogryn (1970) presented some of the first analytical work on the brightness temperature of a vertically structured medium with vertical profiles of dielectric constant and thermodynamic temperature. Tsang, Njoku, and Kong (1975) and Wilheit (1978) proposed solutions for the same problem by representing the stratified medium with a number of dielectric layers. Despite the development of analytical tools, however, just a few models have applied them specifically to represent the vertical structure of foam.

Treating foam as a layered medium, Rosenkranz and Staelin (1972) were the first to model the vertical profile of foam dielectric properties. Foam was initially modeled as a series of thin water films of equal thickness uniformly spaced by air strips, which resulted in oscillations in the computed foam emissivity for a specified foam layer thickness. These unnatural oscillations did not appear when the model was modified to simulate a gradual transition from air to seawater by varying the film thicknesses so that the seawater content Q increased linearly from 0 at the boundary adjacent to the air to 1 at the water interface. Though generally successful, the layered-medium approach to modeling foam void fraction profile in depth remains highly idealized. This is especially true when one needs to choose spurious "foam parameters" like the number and thicknesses of thin layers constituting the foam.

Bordonskiy et al. (1978) used various approaches to represent vertically-structured foam layers, including continuous non-uniform profile, layered medium, and a combination of these two. They used measured and modeled depth profiles of water content to obtain continuous smooth transitions of dielectric properties in foam layers with thickness of 10 mm and 1 mm, respectively. To represent dry foam, they used a large number (50–130) of plane parallel layers, each with a constant permittivity obtained using the Maxwell–Garnett mixing rule. Similar to the Rosenkranz and Staelin (1972) case, the layers caused unrealistic oscillations in emissivity.

Raizer and Sharkov (1982), similarly to Bordonskiy et al. (1978), used plane-layered homogenous structure to represent the vertical change of dielectric properties. However, they avoided the pitfalls of emissivity oscillations observed by Bordonskiy et al. (1978) by using smoothly varying, instead of constant, parameters for each of the structure's plane layers. For thin monolayers of bubbles, they used a continuous dielectric constant profile $\varepsilon_f(z)$ represented by a hyperbolic tangent. For the case of thick foam layers, they obtained a continuous dielectric constant profile by choosing linear dependence of the bubble radius with depth $\varepsilon_f[a(z)]$. Raizer (2007) provided further details on this technique.

2.4.2. Modeling the scattering in sea foam

Volume scattering in a medium is computed using either rigorous solutions of Maxwell equations (the wave approach) or RT theory (the intensity approach) (Ulaby et al., 1986, Chapter 13). Ulaby et al. (1986) summarize the advantages and disadvantages of each of these approaches. Methods based on the wave approach are more mathematically

rigorous and account explicitly for scattering losses. However, to obtain practical results, they employ various approximations, one of which is ignoring multiple incoherent scattering. The intensity approach allows implicit modeling of multiple scattering effects. Ulaby et al. (1986) concluded that, in spite of its limitations (e.g., it ignores diffraction effects), the "intensity approach seems to be the most practical for computing incoherent multiple scattering." Indeed, zero-th and first order solutions of a RT model are customary for foam emissivity investigations (Dombrovskiy, 1979; Dombrovskiy & Raizer, 1992; Droppleman, 1970; Raizer and Sharkov, 1982; Wilheit, 1978; Zhang et al., 2002).

As mentioned in Section 2.1, sea foam is a medium densely packed with scatterers. Experiments have shown that the classical assumption of independent scattering is not valid for dense media (Ishimaru & Kuga, 1982). Tsang and co-workers have systematically investigated scattering in dense media (Tsang, Mandt, & Ding, 1992; Zurk, Tsang, Ding, & Winebrenner, 1995), extending RT theory with equations for Dense Media Radiative Transfer (DMRT) (Tsang, 1992) and applying it to passive remote sensing of snow (Tsang, Chen, Chang, Guo, & Ding, 2000). The applicability of dense media theory to modeling foam emissivity has also been tested. Guo et al. (2001) used DMRT based on the quasi-crystalline approximation to obtain brightness temperatures due to foam at 19 GHz and 37 GHz. Chen et al. (2003) computed the attenuation due to absorption and scattering in densely packed bubbles with Monte Carlo simulations of solutions of Maxwell's equations and then calculated the foam emissivity with DMRT at 10.8 GHz and 36.5 GHz. Combining DMRT equations based on Monte Carlo simulations and a rough foam–water boundary, Zhou et al. (2003) investigated foam emissivity and brightness temperature for all four Stokes parameters at 10.8 GHz, 19 GHz, and 36.5 GHz.

2.4.3. Modeling the thickness distribution of sea foam

In the open ocean, sea foam characteristics vary greatly both spatially and temporally. A variety of meteorological and oceanographic conditions over the globe create sea foam with a range of values for its characteristics. The evolution of foam patches, initially created under specific meteorological and environmental conditions, also leads to a range of values for foam properties. We observe these spatial and temporal variations in two planes: horizontal, expressed as variability of the whitecap fraction; and vertical, expressed as a distribution of foam layer thicknesses. Therefore, whitecap fraction W and foam thickness distribution $p(t)$ are the two variables which can introduce effects that various environmental conditions and lifetime stages of the sea foam have on the brightness temperature due to foam T_{Bf}.

Because W has been extensively studied [see Anguelova and Webster (2006) for references], it is straightforward to account for the influence of environmental factors (e.g., wind speed) in most of the published foam emissivity models by using $T_{Bf}(U) = W(U) \cdot T_s \cdot e_f$. In such a representation, however, e_f remains static in the sense that it does not change either with any environmental variable or with the lifetime stage of the foam layer. This is especially true for empirical models (Section 2.3), in which a specific e_f value is obtained for a set of sensor variables (frequency, polarization and incidence angle). In physical models, e_f involves medium parameters (bubbles or foam layer characteristics), which, though varying with at least wind speed in the most general case, are usually taken as fixed, chosen values. Until now, only two works, those of Dombrovskiy and Raizer (1992) and Reul and Chapron (2003), have addressed the possible variations of T_{Bf} caused by variations of e_f.

Dombrovskiy and Raizer (1992) represented e_f as a varying, dynamic variable by recognizing that various emissivity values are associated with various foam layer thicknesses. Their approach is to average the brightness temperatures due to a range of thicknesses over a Gaussian distribution of thicknesses using $T_{Bf}(t) = T_s \int_{t'} e_f(t')\ p(t')\ dt'$.

Reul and Chapron (2003) proposed another approach for the horizontal and vertical variability of sea foam. The authors developed expressions for characteristic thicknesses of dynamic and static foam (their Eqs. 27 and 30) and used those to obtain foam fraction $W(U, \overline{\delta})$ with average thickness $\overline{\delta}$ at a given wind speed and correction factors for atmospheric stability. The Reul and Chapron (2003) model predicts globally-averaged foam-layer thickness of less than 3.5 cm for decaying whitecaps and less than 1 cm for active ones. These values, though contrary to the expectations due to weighting with the respective areas of active and residual foam cover, compare well with experimental data for foam thickness (Reising, Asher, & Rose, 2002). The foam thickness histogram reported by Reising et al. (2002) does not consider active and decaying whitecaps separately, but also peaks near 3.3 cm and 1.3 cm.

3. Description of the proposed foam emissivity model

The review in Sections 2.3 and 2.4 shows that none of the previous foam emissivity models addresses all the requirements listed in Section 2.2. We believe that it is not necessary to deal with every single requirement if a simplified model can account reasonably well for the main physical features of foam and the unique properties of the major radiative processes in it. Here we justify the emphasis on some requirements and the assumptions we made to simplify others. To make valid assumptions and simplifications, we investigated the dielectric properties of, and the radiative process in, vertically structured foam layers in a series of papers (Anguelova, 2008; AG11; AG12). We use the results of these studies in the following sections.

3.1. Model assumptions and choices

The salient characteristics of surface foam layers (Section 2.1)—vertical stratification of properties and dense packing of bubbles—determine the modeling of the foam vertical profile and the foam losses via both absorption and scattering as the two main requirements to be addressed. These requirements cannot be fulfilled with an empirical model formulated in terms of only sensor variables (e.g., Stogryn, 1972). Instead, they demand a physical model involving medium properties of sea foam (e.g., Droppleman, 1970). The claim that the vertical variations of foam dielectric properties and associated radiative processes make sea foam an exceptional emitter (AG12, Section 5.1) further emphasizes the importance of the medium variables to the modeling of e_f. We, therefore, work with a physical model, which involves both sensor and medium variables.

The decision to use a physical model poses the immediate question of which set of medium variables to use, the micro- or macroscopic set. The modeling of the vertical profile and the volume scattering in foam requires the use of many microscopic foam characteristics (Dombrovskiy & Raizer, 1992; Raizer, 2007; Raizer and Sharkov, 1982). However, the values of these microscopic variables are not well established because few experiments measuring $r(z)$, $w(z)$, $N(z)$, etc. in foam layers have been reported, only those of Militskii, Raizer, Sharkov, and Etkin (1978) and Camps et al. (2005), both in controlled conditions and with artificial foam. The reason for the scarcity in the literature of observed and reported microscopic data in natural foam layers is that it is difficult to measure them on an undulating sea surface, as opposed to the analogous characteristics of the bubble plumes below (Lewis & Schwartz, 2004, Section 4.4; Leifer & de Leeuw, 2006). The uncertainty of the microscopic variables affects the accuracy of the foam emissivity model (Anguelova, 2008).

A viable alternative is to model e_f in macroscopic terms, namely void fraction profile $f_a(z)$ and foam layer thickness t. Admittedly, there are not many measurements of either $f_a(z)$ or t (AG11, Sections 2.4 and 2.5). However, by using macroscopic instead of microscopic characteristics, we limit the number of variables that may introduce uncertainty in the model. Meanwhile, this choice does not restrict the modeling of foam dielectric properties essential for foam emissivity, such as foam skin depth. The rationale for this claim is the finding of Anguelova and Gaiser (AG11, Section 4.4.2) that some features imposed on foam mechanical structure by foam microscopic characteristics can be expressed, and

eventually accounted for, in terms of macroscopic characteristics. In other words, because of a connection between the micro- and macroscopic sets, the relationship between the mechanical and dielectric properties of foam is captured, no matter which set of mechanical characteristics is used.

Renouncing the use of microscopic quantities precludes explicit modeling of the scattering losses in foam. Therefore, working with f_a and t alone, we simplify the model by forgoing one of the two major requirements for modeling e_f. Such a simplification is well justified because a review of published observational and modeling results (Anguelova, 2008, Section 2.3) and analysis of volume scattering in vertically structured foam layers (AG11; AG12) show that at the considered frequencies the scattering in sea foam is weak and the absorption losses dominate in foam. We thus give priority in our emissivity model to the requirement for the foam vertical profile and simplify the requirement for attenuation in foam via both absorption and scattering by accounting for the scattering implicitly.

Accounting for scattering implicitly is achieved with the incoherent approach (Ulaby et al., 1986, Section 18), which is applicable for a weakly scattering medium with low single-scattering albedo, $a = k_s/k_e \ll 1$, but not zero (k_s and k_e are the scattering and extinction coefficients, respectively). In addition, this approach better reflects the loss of phase coherence in a slightly scattering medium, thus avoiding the emissivity oscillations as a function of foam thickness observed by Droppleman (1970).

In addition to volume scattering in foam, we also simplify the consideration of foam surface scattering. Namely, we model the air–foam and foam–water boundaries as plane, rather than irregular, rough surfaces. The rationale for this choice is the investigation of Anguelova and Gaiser (AG12). Comparing estimates of the Fraunhofer criterion for surface smoothness (Ulaby, Moore, & Fung, 1982) to the standard deviation of the surface height due to whitecaps, Anguelova and Gaiser (AG12) have shown that the foam layer boundaries could indeed be rough at some of the considered frequencies. This roughness, however, is not enough to make the surface scattering in foam significant because analysis of the refractive index of foam with various void fractions shows small dielectric contrasts between dry or wet foam and the adjacent medium, air or seawater (AG12). Although it is weak, surface scattering could become important because of the cumulative effect of multiple reflections at the foam layer interfaces. It could also be important when wet foam forms an interface with air (e.g., decaying whitecaps) or dry foam with seawater. To accommodate these expectations, we decided to not fully dismiss the surface scattering of foam and account for multiple reflections at the foam boundaries, but to ignore the roughness of these boundaries.

Because of the mixing during the breaking process, we assume that foam thermodynamic temperature T_f does not change significantly or abruptly over the foam layer depths in which we are interested, from millimeters up to a few centimeters (AG11). Measurements of breaking waves with an infrared technique (Jessup, Zappa, Loewen, & Hesany, 1997) have shown that foam thermodynamic temperature is the same as that of the bulk seawater and thus support our assumption.

Overall, our foam emissivity model, formulated in terms of macroscopic foam characteristics, applies the incoherent approach to a weakly scattering medium with a vertically structured permittivity profile. Checking our choices against the model requirements listed in Section 2.2, the elements of our model are as follows:

- Macroscopic foam characteristics: void fraction f_a and foam layer thickness t;
- Foam with vertically inhomogeneous constitutive parameters, i.e., depth profile of foam dielectric constant $\varepsilon_f(z)$ through a continuous void fraction profile $f_a(z)$.
- Foam with vertically homogenous physical temperature, i.e., constant temperature profile in foam layer depth equal to that of seawater, $T_f(z) = const = T_s$.
- Zero-th order solution of RT equation, i.e., no scattering, denoting $k_s = 0$ and $k_e \equiv k_a$, the incoherent approach.
- Multiple reflections and transmissions at the air–foam and foam–water boundaries.
- Plane air–foam and foam–water boundaries described with Fresnel specular reflectivity.
- A distribution of foam layer thicknesses.

In essence, our foam emissivity model could be considered as a next step in the following sequence of models: (i) the coherent approach with a constant permittivity profile (Droppleman, 1970); (ii) the incoherent approach with a constant permittivity profile (Ulaby et al., 1986, Eq. 18.41); and (iii) the incoherent approach with a stratified permittivity profile (this model). When using a void fraction that is constant in foam depth, our model replicates the incoherent approach demonstrated by Ulaby et al. (1986, their Figs. 18.27 and 18.28).

3.2. Vertical profiles of sea foam properties

3.2.1. Void fraction profile

Considering that the vertical structure of the foam layer is the most important feature in our model, we need to first decide how to model the foam void fraction profile $f_a(z)$ in the layer thickness t. The main choices to be made are the profile shape and the profile range, i.e., the upper and lower limits of $f_a(z)$.

Anguelova and Gaiser (AG11, Section 3.1) surveyed the available information and identified plausible functional forms for $f_a(z)$ (from linear to hyperbolic tangent), which represent a host of profile shapes, some more suitable for dry foam and others for wet foam. Assuming monotonic change in void fraction with depth as presented by Camps et al. (2005, Fig. 9) to be more realistic than those for soap foam (Bordonskiy et al., 1978, Fig. 1), and considering that most oceanographic data for bubble plumes support an exponential change in depth (AG11, Section 2.4), we choose to use an exponential void fraction profile:

$$f_a(z) = a_V - m \cdot e^{b_V z} \tag{1a}$$

$$a_V = \mathrm{v}_{af} + m \tag{1b}$$

$$b_V = \frac{1}{t} \cdot \ln\left(\frac{a_V - \mathrm{v}_{fw}}{m}\right). \tag{1c}$$

Here, m is a parameter that controls the shape of the profile. Coefficients a_V and b_V are determined from the following boundary conditions:

$$f_a(z) = \begin{cases} \mathrm{v}_{af} & @z = 0 \\ \mathrm{v}_{fw} & @z = t \end{cases} \tag{2}$$

where v_{af} and v_{fw} are the void fractions at the air–foam and foam–water boundaries (the upper and lower limits of $f_a(z)$, respectively). Following Anguelova (2008), we cover the full range of possible void fraction values by choosing $\mathrm{v}_{af} = 99\%$ and $\mathrm{v}_{fw} = 1\%$. In this way, we aim to encompass whitecaps in various lifetime stages (active and residual) and under various conditions (low and high wind speeds). We rescale the same range of f_a values (from v_{af} to v_{fw}) for various foam layer thicknesses t by recalculating the coefficient b_V (Eq. 1c).

Fig. 1 shows the variation of the air content in the depth of a 1-cm thick foam layer $f_a(z)$ following an exponential profile ($m = 1$, solid curve). Rescaling of $f_a(z)$ for t of say 0.2 cm or 10 cm preserves the f_a shape. Changes of the f_a shape can be achieved by varying the parameter m. With values $m > 1$ (dashed curve), we can closely represent linear $f_a(z)$ (gray dashed curve). With $m < 1$ (dash-dotted curve), we can approach a combined profile (gray dash-dotted curve) involving constant and linear portions which represents well foam layers with more air (dry foam) (see details in AG11, Section 3.1). Unless otherwise noted, all results here are illustrated with the shape corresponding to $m = 1$.

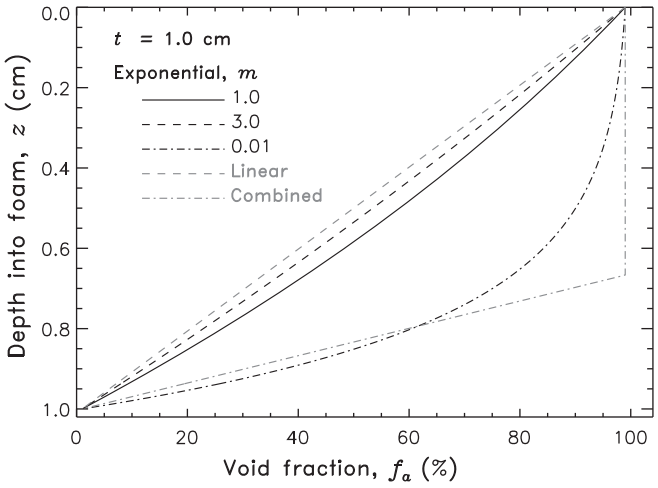

Fig. 1. Exponential void fraction profile $f_a(z)$ in foam layer with thickness $t = 1$ cm; $z = 0$ is the air–foam interface, $z = 1$ cm is the foam–water interface. If t changes, the shape of $f_a(z)$ is preserved. Parameter m changes the shape of $f_a(z)$: $m = 1$ (solid curve), $m = 3$ (dashed curve), $m = 0.01$ (dash-dotted curve). Shown for reference are linear $f_a(z)$ (gray dashed curve) and combined (constant + linear parts) profile (gray dash-dotted curve).

Previous discussions demonstrate that any of our choices here could be challenged simply because there is not enough observational evidence to pinpoint the best choices. Analysis of expected variations of the foam skin depth, and thus foam emissivity, shows that the choice of an exponential profile $f_a(z)$, based on the currently available information, is reasonable (AG11, Section 4.4). Still, for full characterization of the model, Section 5.1.1 investigates the magnitude of e_f variations when the upper or lower limits of the f_a profile, as well as its shape, are varied.

3.2.2. Permittivity profile

The vertical void fraction profile $f_a(z)$ of a foam layer is the principal cause for the variations of the complex dielectric constant (permittivity) $\varepsilon_f(z) = \varepsilon'_f(z) - i\varepsilon''_f(z)$ within the foam layer thickness. The scattering simplification (Section 3.1) allows us to use a classical mixing rule to compute ε_f. In such a mixing rule, the imaginary part of the permittivity ε''_f represents pure absorption in foam and does not involve an additional term accounting explicitly for scattering losses. The main requirement for the mixing rule, therefore, is to predict well the foam dielectric constant over the full range of void fraction values, from 0 to 1.

Many mixing rules for heterogeneous systems have been proposed (Sihvola, 1999). The question is which one is most pertinent for describing foam characteristics and behavior. To this end, Anguelova (2008) investigated the applicability of a group of classical mixing rules for predicting ε_f, namely the Maxwell–Garnett (MG), Polder–van Santen (PS), coherent potential, Looyenga (or cubic) (Lo), and Refractive (or quadratic) (Re) models. The performance of each permittivity model was analyzed according to three criteria: (i) how well a permittivity model deals with a wide range of void fractions; (ii) how well a permittivity model meets the boundary conditions at the air–foam and foam–water interfaces; and (iii) how the choice of a permittivity model affects estimates of emissivity and brightness temperature due to foam. Taking into account the outcomes of the three criteria, Anguelova (2008) ranked the suitability of the considered models, except for the coherent potential, as: 1) Refractive model; 2) Looyenga model; 3) Polder–van Santen model; 4) Maxwell–Garnett model.

Following these results, we use the Refractive model (quadratic mixing rule):

$$\varepsilon_f = \left[f_a + (1 - f_a)\varepsilon^{\frac{1}{2}}\right]^2. \quad (3)$$

In Eq. (3), ε is the dielectric constant of seawater calculated with a double Debye model (Stogryn, 1997). Fig. 2 shows the real (black curves) and imaginary (gray curves) parts of ε_f as a function of void fraction at three frequencies (panels a–c) at fixed seawater temperature $T_s = 20$ °C and salinity $S = 34$ psu. See Anguelova (2008) for extended discussion of the effect of T_s and S on ε_f and Section 5.1.2 for the translation of these ε_f variations into variations of e_f. We show in Fig. 2 the

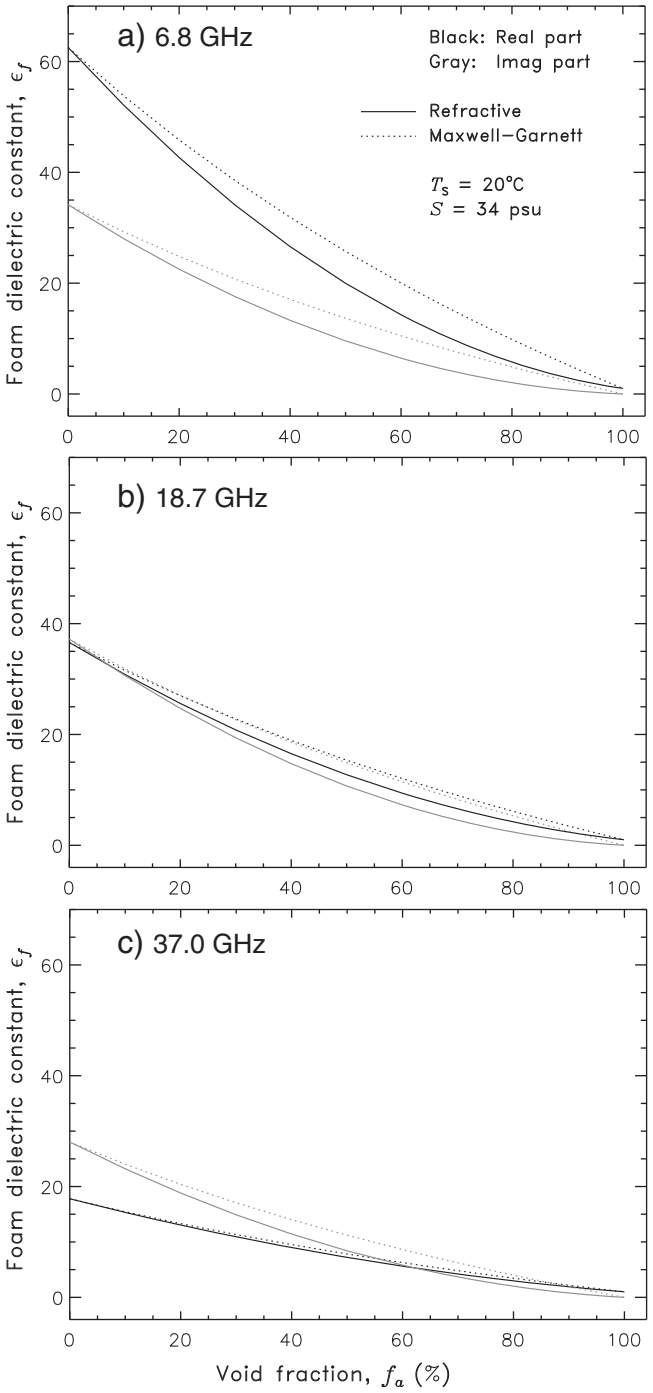

Fig. 2. Complex dielectric constant of sea foam obtained with the refractive mixing rule as a function of foam void fraction $\varepsilon_f(f_a)$ for three frequencies at fixed seawater temperature $T_s = 20$ °C and salinity $S = 34$ psu at frequency of: a) 6.8 GHz; b) 18.7 GHz; c) 37.0 GHz. Black curves show the real part of ε_f; gray curves show imaginary ε_f. Foam permittivity ε_f obtained with the classical Maxwell–Garnett formula (dotted curves) is given for comparison.

difference between the predictions of the quadratic mixing rule and those obtained with the classical Maxwell–Garnett formula (dotted curves) employed previously (Droppleman, 1970; Odelevskiy, 1951; Troitsky, 1962; Wentz, 1974).

3.2.3. Propagation and losses in foam depth

The refraction angle in foam is determined from Snell's law, but to accommodate changes in foam depth from a lossless to a lossy medium, the propagation constant of the transmitted wave is determined by both its attenuation and phase factors. Thus, for radiation incident at an incidence angle θ onto vertically structured foam, the refraction angle is (Ulaby et al., 1981, Section 2–8):

$$\theta_f(z) = \arctan\left\{\frac{\sqrt{2}\ k_0\ \sin\theta}{\left[\left(p^2+q^2\right)^{1/2}+q\right]^{1/2}}\right\} \tag{4a}$$

where $k_0 = 2\pi/\lambda_0$ is the radiation wave number in air. Parameters p and q have the form (note that parameter p here is different from the thickness distribution $p(t)$ introduced in Section 2.4.3):

$$\begin{aligned} p(z) &= 2\alpha\beta \\ q(z) &= \beta^2-\alpha^2-k_0^2\sin^2\theta \end{aligned} \tag{4b}$$

and use attenuation and phase factors (Ulaby et al., 1981, p. 67), respectively:

$$\begin{aligned} \alpha(z) &= k_0\left|\mathrm{Im}\left\{\sqrt{\varepsilon_f(z)}\right\}\right| \\ \beta(z) &= k_0\mathrm{Re}\left\{\sqrt{\varepsilon_f(z)}\right\}. \end{aligned} \tag{4c}$$

The vertical inhomogeneity leads to a vertically non-uniform extinction coefficient of foam: $k_{ef}(z) = k_{af}(z) + k_{sf}(z)$. Here $k_{sf}(z) = 0$ because we do not consider scattering losses in foam explicitly (Section 3.1). The extinction coefficient therefore involves only the absorption losses determined by the attenuation factor $k_{ef}(z) \equiv k_{af}(z) = 2\cdot\alpha(z)$. The foam optical depth (or integrated attenuation) $\tau_{f\theta}$ along a path formed by the changing incidence angle $\theta_f(z)$ in a foam layer of thickness t then is:

$$\tau_{f\theta}(0,t) = \int_0^t k_{ef}(z)\cdot\sec\theta(z)\ dz = 2\int_0^t \alpha(z)\cdot\sec\theta(z)\ dz. \tag{5}$$

The total loss factor L_f of the foam layer becomes $L_f(\theta,t) = e^{\tau_{f\theta}}$.

3.3. Radiometric signal from a foam-covered surface

For a radiometer observing a system involving a foam layer floating on seawater surface at incidence angle θ, the measured brightness temperature $T_{B\ obs}$ consists of atmospheric radiation reflected in the direction of the radiometer T_{Br} and radiation emitted from the foam layer and the water below it (T_{Bl} and T_{Bw}, respectively):

$$T_{B\ obs} = T_{Br} + T_{Bl} + T_{Bw} = T_{Br} + T_{BlU} + T_{BlD} + T_{Bw}. \tag{6}$$

As Eq. (6) shows, T_{Bl} comprises two terms: radiation emitted upward T_{BlU} and radiation emitted downward and partially reflected by the foam–water boundary toward the air–foam boundary T_{BlD}. The analytical expressions represented by the terms in Eq. (6) follow the presentation of the incoherent approach (Ulaby et al., 1981, Section 4–14.2) and are given in the Appendix A.

3.4. Distribution of foam thicknesses

To account for the simultaneous presence of foam in various stages of whitecap lifetime, we integrate $T_{B\ obs}$ in Eq. (6) over a distribution of foam layer thicknesses following Dombrovskiy and Raizer (1992) and obtain the brightness temperature due to foam as:

$$T_{Bf} = \int_{t_{min}}^{t_{max}} T_{Bobs}(t)p(t)dt. \tag{7}$$

There are two questions to resolve here: (i) What range (t_{min}, t_{max}) of foam layer thicknesses should be considered, and (ii) what probability density function $p(t)$ should be used for the thickness distribution.

To be able to reliably cover thin foam streaks of decaying foam as well as active foam generated by very high winds at the frequencies we use (up to 37 GHz), we establish minimum and maximum foam layer thicknesses as follows:

$$\begin{aligned} t_{\min} &\geq \lambda_{0@37\ \mathrm{GHz}}/20 \approx 0.04\ \mathrm{cm} \\ t_{\max} &\leq 5\ \lambda_{0@6.8\ \mathrm{GHz}} \approx 25\ \mathrm{cm}. \end{aligned} \tag{8}$$

This range is in agreement with the foam layer thicknesses expected to be observed in open ocean (Section 2.1).

In resolving the second question, we realize that we do not expect or seek a symmetric probability over the range of foam thicknesses. On one hand, high winds forming very thick foam layers are rare. Yet, the presence of occasional, thick foam layers should be allowed. On the other hand, extremely thin foam streaks would not have the large effect on brightness temperature that more typical active and residual whitecaps would. These expectations call for a positively skewed distribution which features a peak of probable values clustered at relatively low, but not at the lower limit of the t range and a long tail toward large t values. Log-normal distributions have such features.

The shape and the scale of the probability density function $p(t)$ are readily adjusted with the statistical parameters of a realization of t values, the mean μ and the standard deviation σ. For a realization of thicknesses with values from t_{min} to t_{max}, we choose μ and σ values so that the resulting log-normal density distribution $p(t)$ peaks at thickness of approximately 3.5 cm and has a long tail of non-zero probability up to t_{max} (Fig. 3). The shape of $p(t)$ is physically expected and also consistent with the results of Reul and Chapron (2003) and the measurements reported by Reising et al. (2002) (Section 2.4.3). Section 5.1.3 quantifies the variations of e_f values when μ and σ vary so that $p(t)$ peaks at different t.

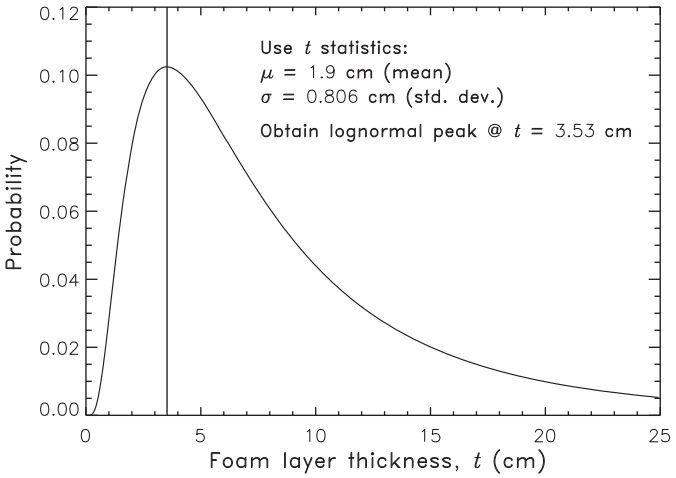

Fig. 3. Log-normal distribution (weighting coefficients) $p(t)$ of a realization of thicknesses with values from t_{min} to t_{max} (see Section 3.4). The mean μ and the standard deviation σ of the t realization determine that the peak probability occurs at a thickness of ~3.5 cm and that there is a long tail up to t_{max}.

4. Results

The following sections present results of our foam emissivity model. The computations use an exponential void fraction profile $f_a(z)$ in foam layer depth with upper (air–foam) and lower (foam–water) limits of 99% and 1%; refractive mixing rule for the foam permittivity ε_f at seawater temperature $T_s = 20$ °C and salinity $S = 34$ psu, and foam layer thicknesses covering the range from 0.04 cm to 25 cm and weighted with a log-normal probability density $p(t)$ peaking at $t = 3.53$ cm when using statistics $\mu = 1.9$ cm and $\sigma = 0.81$ cm. The foam emissivity e_f is calculated for all five WindSat frequencies (Gaiser et al., 2004) and L band; however, results are shown for 6.8 GHz (always with dash-dotted curves), 18.7 GHz (solid curves) and 37 GHz (dashed curves).

4.1. Foam parameters

Fig. 4 shows the vertical profile of the foam dielectric constant $\varepsilon_f(z)$ for a layer with thickness $t = 2$ cm at three frequencies. Black and gray curves represent the real $\varepsilon_f' = \mathrm{Re}\{\varepsilon_f(z)\}$ and imaginary $\varepsilon_f'' = \mathrm{Im}\{\varepsilon_f(z)\}$ parts of foam permittivity. At the surface of the foam layer ($z = 0$), ε_f is that of the air ($\varepsilon_f' = 1$, $\varepsilon_f'' = 0$). Within the foam depth ($z > 0$), ε_f increases gradually reaching the permittivity of seawater at $z = t$ corresponding to each F. For 6.8 GHz, the relationship $\varepsilon_f'' < \varepsilon_f'$ holds for the entire foam thickness, which indicates that the losses remain small throughout the foam layer. This is expected because at this frequency the scattering is negligible and the water content of the foam layer is insufficient for strong absorption (AG11). For 18.7 GHz, the same observation holds true almost to the bottom of the foam layer, where eventually $\varepsilon_f'' \approx \varepsilon_f'$. This suggests that the losses in foam at this frequency are significant only for very wet foam. Finally, for 37 GHz, we see that ε_f'' becomes larger than ε_f' approximately in the middle of the foam layer, which means that the losses, mostly absorptive, are significant. In Fig. 5, a plot of the vertical profile of the absorption coefficient $k_{af}(z)$ (Section 3.2.3) shows these differences in the attenuation, and therefore emission, in foam depth at various frequencies: largest at 37 GHz and smallest at 6.8 GHz.

Fig. 6 shows the profile of the refraction angle in the foam depth $\theta_f(z)$ for the same three frequencies. For an initial incidence angle $\theta = 53°$ at the air–sea interface, the transmitted wave propagates downward into the foam at an angle that decreases with depth and eventually intersects the foam–seawater interface at an angle of approximately 5° to 7°, almost normal incident angle. This angle decreases to ≤2–3° when the initial angle $\theta < 53°$. The refraction angle decreases with frequency, as expected from the classical electromagnetic theory. However, the close clustering of the curves in Fig. 6 at the three frequencies attests to relatively weak frequency dependence of the changes of θ_f with depth in the foam.

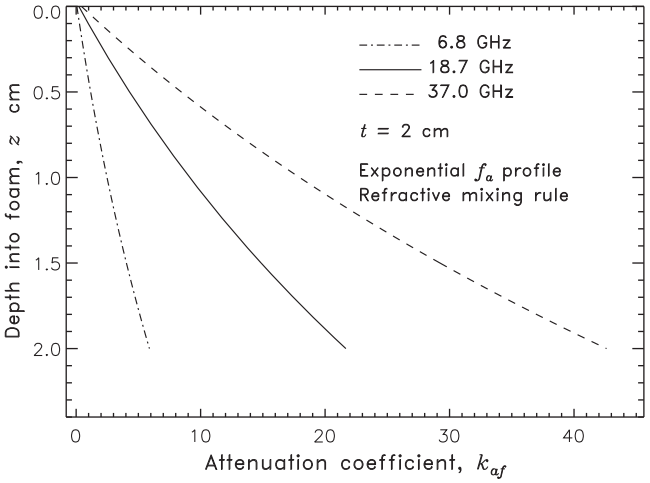

Fig. 5. Vertical profile of the absorption coefficient with depth in the foam $k_{af}(z)$ (see Section 3.2.3) for a layer with thickness $t = 2$ cm at three frequencies: 6.8 GHz (dash-dotted curves), 18.7 GHz (solid curves), and 37 GHz (dashed curves).

4.2. Foam emissivity

Here we present the model results for two major factors determining foam emissivity: foam layer thickness $e_f(t)$ and incidence angle $e_f(\theta)$.

4.2.1. Thickness dependence of foam emissivity

The results of our emissivity model quantify the qualitative findings of Anguelova and Gaiser (AG11). Analyzing foam skin depth for various thicknesses, Anguelova and Gaiser identified conditions under which foam would be distinguished from the surrounding seawater (AG11, Section 4.1.1) and noted that the thermal emission of foam-covered surfaces can be formed by the foam layer itself or by the coupled foam–seawater system (AG11, Section 4.2.1). The authors acknowledged the role of the layer thickness in determining the emissivity signal by introducing the concept of radiometrically nominal, radiometrically thick,

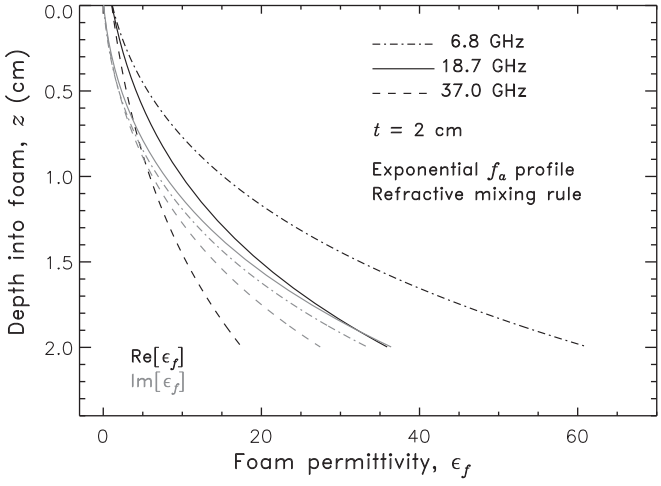

Fig. 4. Vertical profile of the foam dielectric constant with depth in the foam $\varepsilon_f(z)$ obtained with an exponential void fraction profile $f_a(z)$ (see Section 3.2.1) and refractive mixing rule (see Section 3.2.2) for a layer with thickness $t = 2$ cm at three frequencies: 6.8 GHz (dash-dotted curves), 18.7 GHz (solid curves), and 37 GHz (dashed curves). Black and gray curves represent the real $\varepsilon_f' = \mathrm{Re}\{\varepsilon_f(z)\}$ and imaginary $\varepsilon_f'' = -\mathrm{Im}\{\varepsilon_f(z)\}$ parts.

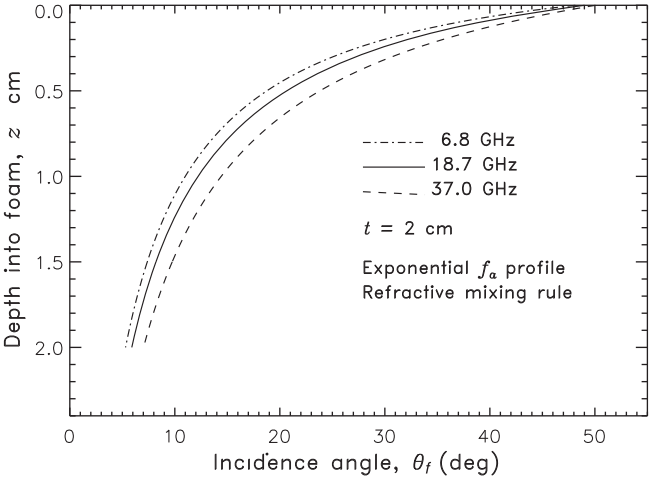

Fig. 6. Vertical profile of the refraction angle with depth in the foam $\theta_f(z)$ at three frequencies: 6.8 GHz (dash-dotted curves), 18.7 GHz (solid curves), and 37 GHz (dashed curves). The initial incidence angle at the air–sea interface ($z = 0$) is $\theta = 53°$.

and radiometrically thin foam layers. Using this concept, they deduced regimes with expected variations of foam emissivity with layer thickness $e_f(t)$ (AG11, Section 4.2.2 and Table 3). Fig. 7 illustrates these regimes and variations of e_f determined quantitatively and reveals new information about them.

Fig. 7a shows the incoherent total emissivity e_f (black curve) and reflectivity $1 - e_f$ (gray curve) of the foam–seawater system represented with Eq. (A.8a,b) at 18.7 GHz, H polarization, as a function of the foam layer thickness $e_f(t)$. Fig. 7b shows the variations of these two curves over an extended range of emissivity (note the log scale of the y axis). It also shows the terms contributing to the total emissivity, namely upwelling e_{fu} (dashed curve), downwelling e_{fd} (dotted curve), and transmitted e_{ft} (dash-dotted curve) radiation.

The vertical lines in Fig. 7a mark two noteworthy foam thicknesses t_n and t_e. The former is the nominal thickness at 18.7 GHz, $t_n \approx 0.21$ cm introduced by Anguelova and Gaiser (AG11, Table 1). The latter is the crossing point between the emissivity and reflectivity at $t_e \approx 0.009$ cm, new information revealed by the emissivity model. Thickness t_f in Fig. 7b is another key point identified with the emissivity model. At t_f, terms e_{fu} and e_{ft} reverse their relative importance: the transmitted radiation is larger than the upwelling radiation for foam thickness $t < t_f$; the opposite is true for layers thicker than t_f. Thickness t_f is also notable for the relation between terms e_{fu} and e_{fd}: for $t < t_f$, the downwelling radiation has the same trend as that of the upwelling radiation, but at roughly half its magnitude; in layers thicker than t_f, the trend of e_{fd} with t slows down, reaches a broad peak, and then decreases together with e_{ft}. Points t_e and t_n divide the $e_f(t)$ dependence into three regions, each with characteristic behavior of $e_f(t)$. In the following we show that the key thicknesses (t_e, t_f, and t_n) in Fig. 7 delineate the emissivity regimes deduced by AG11.

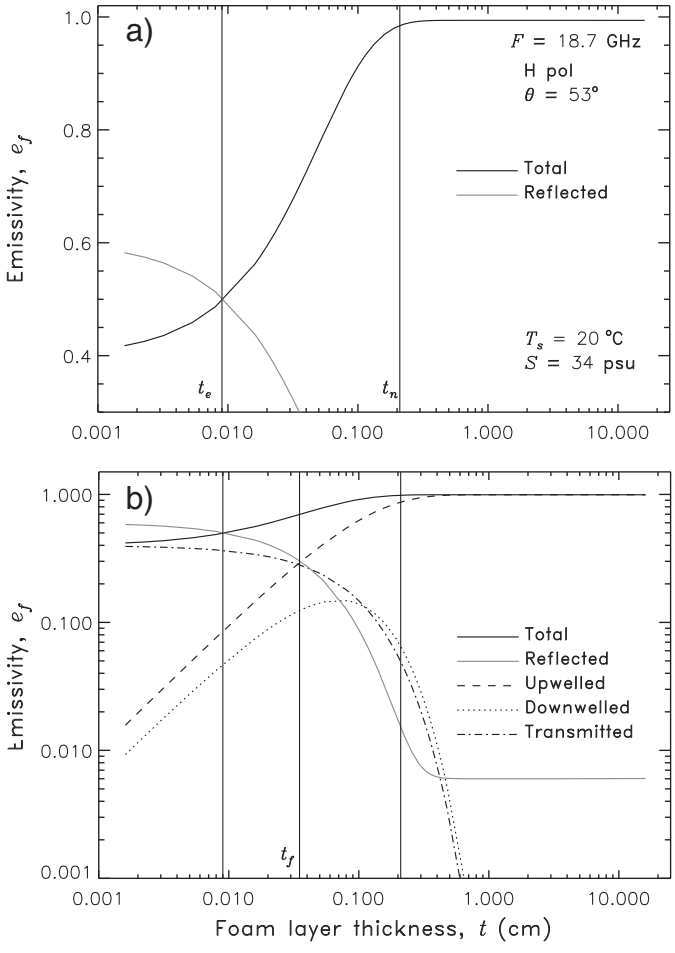

Fig. 7. Dependence of foam emissivity on foam layer thickness $e_f(t)$ for a frequency of 18.7 GHz, H polarization, and an incidence angle $\theta = 53°$ at seawater temperature $T_s = 20$ °C and salinity $S = 34$ psu. a) Total emissivity e_f (black curve) and reflectivity $1 - e_f$ (gray curve); b) terms contributing to the total emissivity — upwelling e_{fu} (dashed curve), downwelling e_{fd} (dotted curve), and transmitted e_{ft} (dash-dotted curve) radiations. The vertical lines denote thicknesses that divide different emissivity regimes from one another (see Section 4.2.1).

We start with foam thickness $t \le t_e$ in Fig. 7a and b. Considering that measured bubble size distributions peak at about 50 μm (Deane & Stokes, 2002), it is conceivable that such thin foam layers formed by such small bubbles may exist. Two observations point out that in this regime foam layers behave as the seawater itself. First, in this region of the $e_f(t)$ curve, foam is more reflective than emissive (gray curve above black curve). Second, the relatively low emissivity is in effect that of the seawater (dash-dotted curve close to black curve) with negligible contributions from upwelling and downwelling radiation within the foam. Foam is distinguished from the surrounding seawater at 18.7 GHz by its increasing emissivity when it is thicker than t_e.

Next, from the definition of the nominal thickness (AG11)—the foam thickness over which a given void fraction profile redistributes the same amount of seawater as that contained in the seawater skin depth for the considered frequency—it is clear that thickness t_n is that at which the emission comes from the foam layer in its entirety. Indeed, Fig. 7b shows that at thickness t_n the main contribution to foam emissivity is from the upwelling radiation in foam with an order of magnitude lower contributions from e_{fd} and e_{ft}. There is little variation in foam emissivity for layer thicknesses larger than t_n, and e_f reaches saturation for $t \gg t_n$. The model thus confirms the deduced e_f variations for radiometrically thick foam layers (AG11, Table 3) for which only a portion of the foam layer suffices to provide the bulk (86%) of the foam emissivity.

Furthermore, the model results help to localize the deduced large variations of e_f associated with radiometrically thin layers (AG11, Table 3) in the range from t_e to t_n (Fig. 7). As defined, radiometrically thin foam layers alone cannot provide the high foam emissivity; rather their emission is reinforced by that of the underlying seawater. Fig. 7b attests to this by showing the relative contributions from foam (e_{fu} and weaker e_{fd}) and seawater (e_{ft}) in this range. The seawater contribution dominates the e_f signal for thickness $t_e < t < t_f$. For $t_f < t < t_n$, the foam layers are increasingly responsible for the foam emissivity. As terms e_{fu} and e_{ft} increase with thickness by an order of magnitude in the t_e to t_n range, various portions of the seawater column and a large range of foam thicknesses participate in the formation of the emissivity signal. This results in large e_f variations.

All trends observed in Fig. 7 for 18.7 GHz are the same for other frequencies. What changes are the exact values of the key foam thicknesses t_e, t_f, and t_n. Anguelova and Gaiser (AG11) explained the mechanism behind this frequency sensitivity to foam thickness and on its basis suggested useful implications for remote sensing of sea foam.

4.2.2. Angular dependence of foam emissivity

The results in Fig. 7 are for H polarization at fixed incidence angle θ of 53°. Fig. 8 demonstrates that the e_f saturation from radiometrically thick foam layers (fixed $t = 1$ cm in panel a and $t = 5$ cm in panel b) is preserved for all incidence angles and all frequencies. It also shows that thick foam layers depolarize the radiation: V polarization (gray curves) has only slightly higher values than H polarization (black curves) for all frequencies, and both polarizations have almost identical trends with θ. Even radiometrically thin foam layers depolarize the radiation (Fig. 8c), but to a different degree for different frequencies. As Anguelova and Gaiser (AG11, Section 4.2.1) anticipated, even mechanically thin layers ($t = 0.05$ cm in Fig. 8c) will saturate the emissivity signal at 37 GHz (dashed curves). Meanwhile, at low frequencies (e.g., 6.8 GHz in Fig. 8c, dash-dotted curves) e_f will approach seawater-like behavior for mechanically thin foam layers.

Fig. 9 shows the effect of using a distribution of foam thicknesses instead of a fixed t value. Once again, the angular dependence of H and V

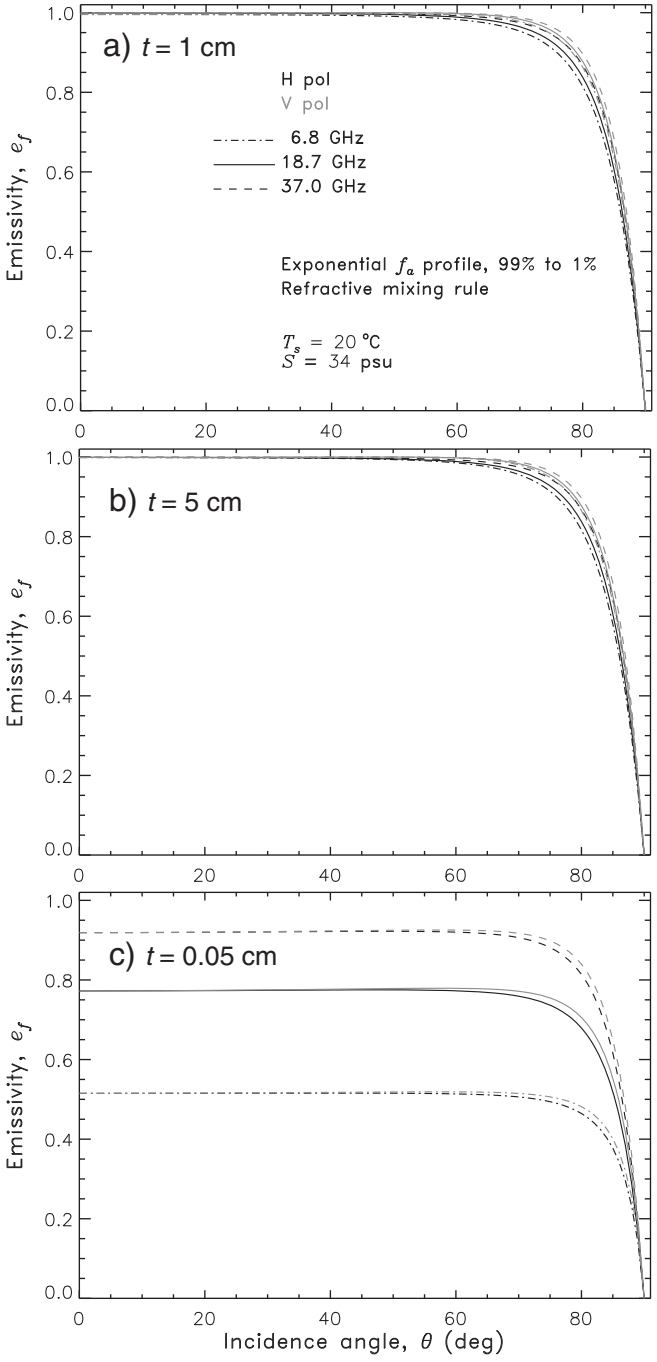

Fig. 8. Dependence of foam emissivity on incidence angle e_f (θ) at three frequencies: 6.8 GHz (dash-dotted curves), 18.7 GHz (solid curves), and 37 GHz (dashed curves) and three fixed thicknesses t: a) t = 1 cm; b) t = 5 cm; c) t = 0.05 cm. Polarizations H (black curves) and V (gray curves).

polarizations is the same, but the maximum emissivity signal is not as close to unity as it is in Fig. 8a and b, but instead it decreases to 0.90–0.95 for θ of at least 70° and up to 78° depending on the frequency.

5. Discussion

In this section we focus our attention on three topics. First, we investigate the sensitivity of our foam emissivity model to the choices of the model input values. Second, we compare the results of our emissivity model to published experimental and modeling data. Finally, these discussions help us to evaluate the performance of our emissivity model and devise possible improvements.

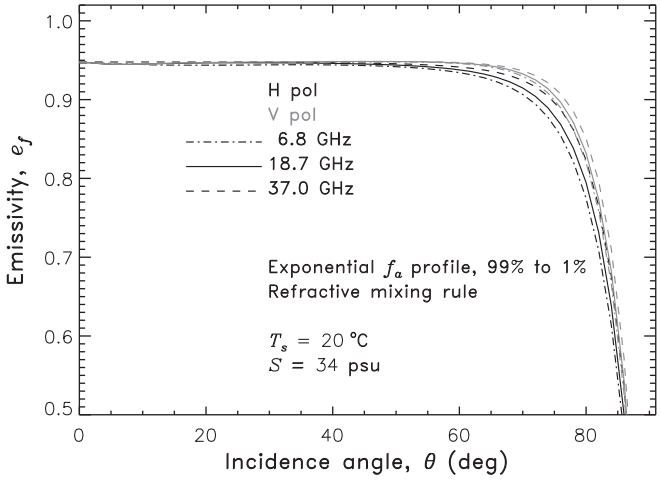

Fig. 9. As Fig. 8 but for a distribution of foam thicknesses instead of fixed t values.

5.1. Model sensitivity to input choices

The main elements of our foam emissivity model, as justified in Section 3.1, are (i) a profile $f_a(z)$ over the full range of void fraction values with an exponential shape (Section 3.2.1); (ii) a refractive mixing rule for the permittivity $\varepsilon_f(z)$ chosen among other mixing rules as most suitable to represent sea foam properties (Section 3.2.2); and (iii) a log-normal probability density function with parameters μ and σ ensuring a probability peak at experimentally observed foam thickness t (Section 3.4). These choices are based on systematic investigation of sea foam properties (Anguelova, 2008; AG11; AG12). Here we discuss the model sensitivity to variations of some parameters and variables in each of these three elements. We quantify the model sensitivity as percent difference of foam emissivity, defined as $\Delta e_f = 100 \cdot |e_{fvar} - e_{fchc}|/e_{fchc}$, where e_{fchc} is the emissivity obtained with the model choices, and e_{fvar} is the emissivity obtained with some variations of the choices.

5.1.1. Variations of the void fraction profile

Once the choice of a vertical profile of foam fraction instead of a constant void fraction in foam depth is justified (Section 3.1), the functional form of representing $f_a(z)$ comes into play. In addition, Anguelova (2008, Section 5.3) noted the sensitivity of e_f to the choice of the upper and lower limits of the profile. Anguelova and Gaiser (AG11, Section 3.3. and 4.2.3) extended this investigation by considering how varying limits of the f_a profile and varying f_a shape affect the foam skin depth. They found that the foam skin depth is affected more by variations in the upper limit of the f_a profile than by changes in its lower limit or its shape obtained using various functional forms. These results for the foam skin depth extend naturally to the foam emissivity.

Fig. 10a shows e_f (θ) for three upper limits of void fraction v_{af} (95%, 85%, and 75%) different from the chosen v_{af} = 99%; the lower limit remains fixed at v_{fw} = 1%, as do all other elements of the model. Fig. 10a shows that decreasing the upper limit of the void fraction profile changes the foam emissivity in two ways. First, the e_f values decrease with decreasing v_{af}, yet they stay much higher than the seawater emissivity. That is, though not as clearly as for dry foam, the emissivity of wet foam is readily distinguishable from the seawater emissivity. Second, the depolarizing nature of foam quickly diminishes for $v_{af} \leq$ 95% (dotted curves) as polarization differences in e_f values are observed for such upper limits. That is, only the highest void fractions fully depolarize the emissivity signal. Fig. 10b shows the difference Δe_f between emissivity with a profile with upper limit of 99% and each of the profiles with lower v_{af} in Fig. 10a. These Δe_f curves demonstrate that variations of the upper f_a limit change e_f values for H polarization more than for the V polarization, e.g., e_f H changes by up to about 40% for $\theta < 60°$, while e_f V varies by no more than about 30% for almost the entire θ range.

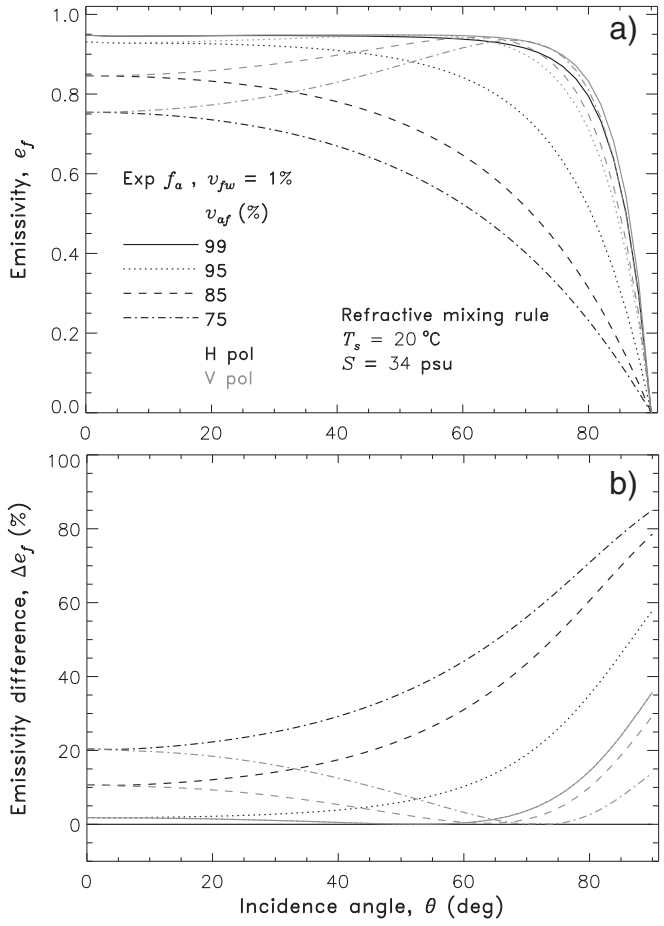

Fig. 10. a) Variations of the emissivity e_f due to changes of the upper limit of the void fraction from 99% to 95% (dotted curve), 85% (dashed curve), and 75% (dash-dotted curve). Polarizations H (black) and V (gray). b) Emissivity difference Δe_f between emissivity with a profile with upper limit of 99% and each of the profiles with lower v_{af} in Fig. 10a.

These observations are for a frequency of 18.7 GHz and remain the same for all other frequencies. Varying the lower limit of f_a from 1% up to 40% at any fixed upper limit does not change the e_f values, Δe_f is $O(10^{-3}\%)$.

Variations of parameter m in the exponential profile above or below unity simulate shapes of f_a which contain more or less air (Fig. 1). In a manner similar to the upper limit variations of f_a, the foam emissivity changes little ($\Delta e_f \ll 1\%$) if the profile contains more wet foam represented with $m > 1$. When the profiles have more dry foam ($m < 1$), Δe_f may change by up to 14% at 37 GHz and by no more than 56% for 6.8 GHz for any θ. Comparison of these Δe_f values with those in Fig. 10b suggests that variations of the upper f_a limit cause the largest variations of e_f.

5.1.2. Variations of the permittivity profile

Anguelova (2008, Section 5.3) investigated in detail the impact of the mixing rule choice on foam emissivity; here we give a brief summary of the results. The choice of the mixing rule is strongly affected by the choice of whether to use it with a constant void fraction value f_a or with a void fraction profile $f_a(z)$. Depending on this choice, $e_f(\theta)$ values differ appreciably for various mixing rules. Specifically, when the MG, Lo, and Re mixing rules are used, $e_f(\theta)$ did not change significantly when employed with a constant f_a value or a f_a profile; meanwhile, $e_f(\theta)$ was substantially affected when the PS rule was used. Overall, the use of a f_a profile instead of a constant f_a value reduced the sensitivity of the emissivity model to the choice of the mixing rule. Based on this and additional criteria (Anguelova, 2008), we find the choice of the refractive mixing rule to be the most suitable one among those studied.

Anguelova (2008, Section 4) showed that seawater temperature T_s and salinity S affect the foam permittivity values. These variations affect in turn the foam skin depth (AG11). Ultimately, variations of T_s and S result in variations of the foam emissivity. Calculations of $e_f(\theta)$ for various T_s (10 °C, 20 °C, and 30 °C) and S (0, 10, 34, 40 psu) values show Δe_f of at most 0.2% and in most cases $\ll 0.2\%$. In other words, most variations of e_f via ε_f come from the choice of mixing rule, not from environmental variables such as SST and salinity.

5.1.3. Variations of the foam thickness distribution

The results in Figs. 8 and 9 indicate that the foam emissivity calculated with the chosen thickness distribution (Fig. 3), which peaks at 3.53 cm, would differ by about 5% from e_f values obtained for a fixed thickness of 3.53 cm. Choosing a fixed value of t of less than 1 cm would lead to a range of Δe_f differences (Figs. 8c and 10), small for low frequencies ($\Delta e_f \sim 4\%$ for 6.8 GHz) and higher for high frequencies ($\Delta e_f \sim 25\%$ for 37 GHz). Varying the peak of the thickness distribution by changing parameters μ (0.3, 1.0, 1.9, 4.0 cm at fixed $\sigma = 0.81$) and σ (0.3, 0.81, 1.0, 2.3 cm at fixed $\mu = 1.9$ cm) leads to Δe_f variations of the same order. Overall, these thickness-induced variations of the foam emissivity are of the same order as, yet smaller than ($\leq$25%), the variations caused by the upper f_a limit.

Overall, our sensitivity study demonstrates that the results of our foam emissivity model are most affected by the choice of the void fraction value at the air–foam interface or, equivalently, by the choice of the profile shape. The influence of the foam layer thickness on the e_f values is tangible, yet somewhat diminished [compared to its effect on foam skin depth (AG11)] because of the use of a distribution of thicknesses. All other parameters and variables in the model lead to much smaller variations of e_f. These results confirm quantitatively the anticipated effectiveness of the upper limit of the f_a profile as a tuning parameter (Anguelova, 2008, Section 5.3.3) for the emissivity of vertically stratified foam.

5.2. Comparison to measurements and other models

In the comparisons, we use the experimental data for the angular dependence of foam emissivity $e_f(\theta)$ reported by Raizer and Sharkov (1982), Rose et al. (2002), and Camps et al. (2005). Each experimental data set has been used to evaluate the performance of previously developed physical models for the microwave foam emissivity (details below). We include these models in the comparisons. For applicable frequencies ($F > 13.4$ GHz), we include also the empirical model of Stogryn (1972). Considering the experimental values as a reference, we quantify the deviations of our model and any other emissivity model from this reference with a root–mean–square (rms) error $\sigma_P = \sqrt{\sum_{i=1}^{n}(e_{f\,Pmod} - e_{f\,Pexp})^2/n}$, where $e_{f\,Pexp}$ and $e_{f\,Pmod}$ are the experimental and model data, respectively, for P (H or V) polarization, for n measurements over the range of incidence angle θ. The rms errors (rmse) σ_H and σ_V for all model-experiment comparisons are listed in Table 1; rmse for our model are reported below (as a fraction or as percentage) and are also given in the figures. For all figures in this section, the experimental data are shown with squares, results of our emissivity model with solid curves, other physical models with dashed curves, and Stogryn's model with dotted curves. Black symbols and curves are for H polarization, and gray is for V polarization.

5.2.1. Rose et al. (2002) experimental data

Rose et al. (2002) performed measurements of artificially generated foam at 10.8 GHz and 36.5 GHz, foam thickness of approximately 2.8 cm, water temperature of 19 °C, and salinity of 10 psu. From analysis of video images, they estimated $f_a = 0.85$ in the center of the foam layer and reasoned that f_a may increase up to 0.95 at the surface of the layer. Rose et al. data are shown in Fig. 11, panel (a) for 10.8 GHz and panel (b) for 36.5 GHz.

Table 1
RMS errors for various models compared to experimental data.

Experiment			Model						
			Other model			Stogryn (1972)		This study	
Source	F (GHz)	t (cm)	Source	σ_H	σ_V	σ_H	σ_V	σ_H	σ_V
Rose et al. (2002)	10.8	2.8	Chen et al. (2003)	0.057	0.018	n/a[a]	n/a	0.011	0.015
	36.5	2.8		0.041	0.021	0.19	0.14	0.015	0.017
Raizer and Sharkov (1982)	35.0	0.1	Raizer and Sharkov (1982)	0.096	0.021	0.12	0.12	0.015	0.019
		1.0		0.010	0.004	0.27	0.19	0.006	0.006
Camps et al. (2005)	1.4	1.7	Dombrovskiy and Raizer (1992)[b]	0.017	0.012	n/a	n/a	0.016	0.016

[a] Stogryn (1972) model is applicable for a frequency range of 13.4 GHz to 37 GHz.
[b] This model is the basis on which Camps et al. (2005) develop their foam emissivity.

Chen et al. (2003) compared the results of their DMRT model (brief description in Section 2.4.2) to Rose et al. values assuming constant $f_a = 90\%$. DMRT model results are also shown in dashed curves in Fig. 11. Fig. 11b includes also e_f values from Stogryn (1972) model shown in dotted curves. As seen in the figure and Table 1, Stogryn's empirical model underestimates the measured e_f values by 14% to 19%.

To find an efficient way of comparing our model results to experimental data, we ran our model at 10.8 GHz with several inputs. The first model run was for the experimental conditions of Rose et al. (T_s and S) with a f_a profile from 95% to 1% with foam thickness fixed at 2.8 cm. With these inputs, our model overestimates e_f by $\sigma_H = 8.5\%$ and $\sigma_V = 6.1\%$. Our previous investigations (Anguelova, 2008; AG11; AG12) suggest that these rms errors can be most effectively minimized by tuning the upper limit v_{af} of the f_a profile. However, before tuning, we performed a second model run with the same f_a profile as above and added a distribution of thicknesses with our chosen parameters (see the preamble of Section 4). The rationale for this model run was that we would like to keep as many of the chosen model elements close to the same as possible before tuning the model with the void fraction. Using the model with the chosen thickness distribution, σ_H decreased to about 4% and σ_V became 1.4%. In the last run, we tuned the model by changing only the upper f_a limit from 95% to 93%. The results (Fig. 11a and Table 1) are $\sigma_H = 0.011$ and $\sigma_V = 0.015$.

The results for 36.5 GHz with the same approach—all model elements in place and tune only v_{af}—are shown in Fig. 11b. Tuning v_{af} to 91%, we

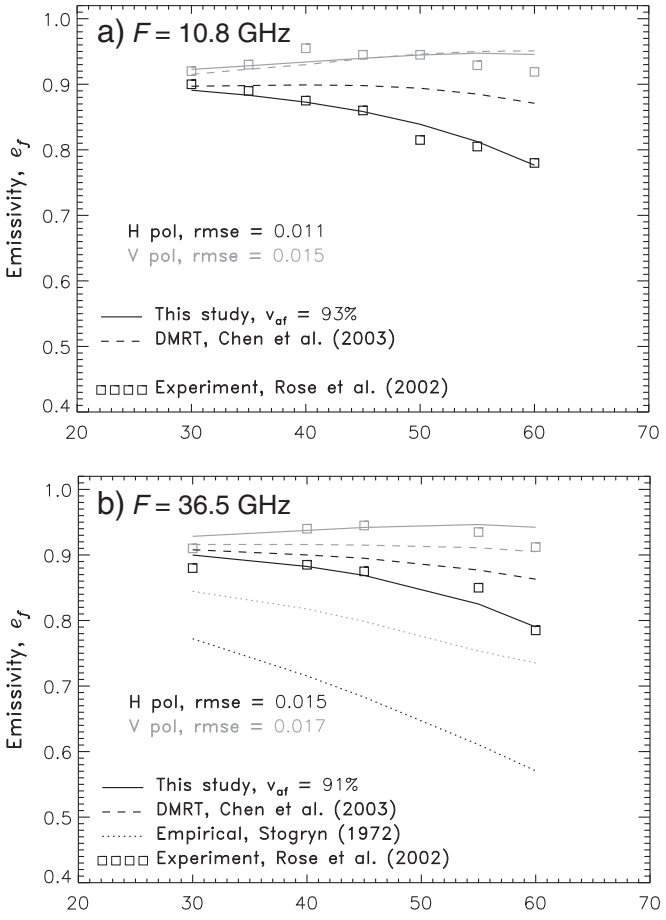

Fig. 11. Comparison of foam emissivity calculated with the model in this study to experimental (Rose et al., 2002, symbols) and model (Chen et al., 2003, dashed curves) foam emissivities at two frequencies: a) 10.8 GHz; b) 36.5 GHz. Emissivity obtained with the empirical model of Stogryn (1972, dotted curves) is also shown in panel b. Black symbols and curves are for H polarization, and correspondingly, gray ones are for V polarization. Details are provided in Section 5.2.1.

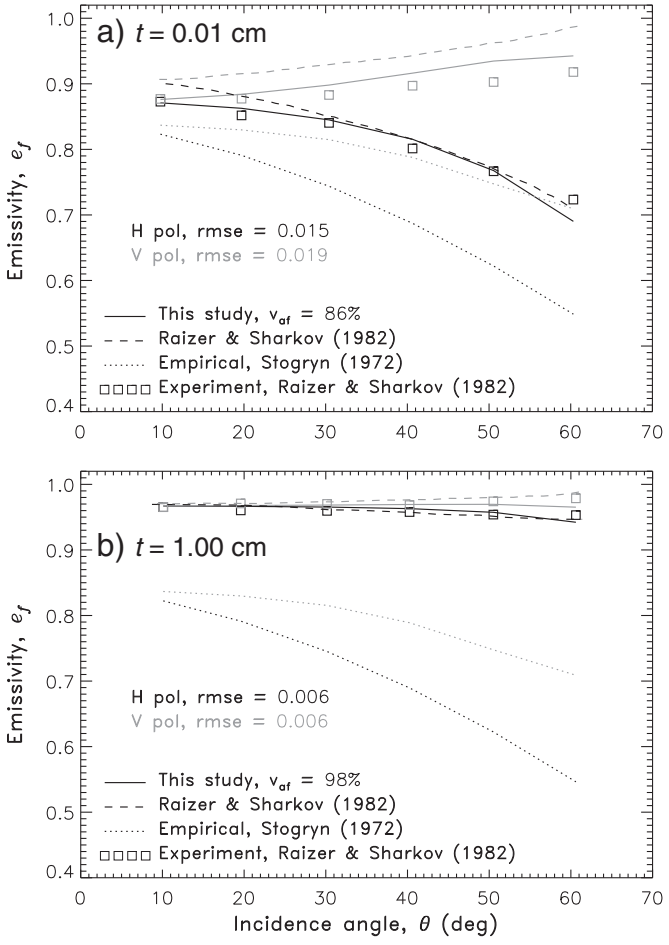

Fig. 12. As Fig. 11 but for experimental and model data of Raizer and Sharkov (1982) at frequency of ~35 GHz for two foam layer thicknesses: a) 0.1 cm; b) 1 cm. Details are provided in Section 5.2.2.

obtain $\sigma_H = 0.015$ and $\sigma_V = 0.017$. As shown in the figure and Table 1, for both frequencies our model performs better than the DMRT model, especially for H polarization.

5.2.2. Raizer and Sharkov (1982) experimental data

Raizer and Sharkov (1982) compare the results of their model (brief description in Section 2.4.1) to experimental data from a series of laboratory measurements (symbols in their Fig. 5). The measurements were made for a wavelength of 0.86 cm (≈35 GHz) and thin (0.1 cm) and thick (1 cm) layers of soap foam ($S = 0$ psu) at $T_s = 27$ °C. Fig. 12 shows the experimental and modeled (model 6 in their Table 2) data for thin (panel a) and thick (panel b) layers. As in Fig. 11, Stogryn's empirical model underestimates the experimental values by 12% to 27% (Table 1).

Using the same approach for comparison as that established for Fig. 11 (all chosen model elements and tunning only of the v_{af} value), our model results for a thin layer (Fig. 12a) reproduce the measured e_f values well when $v_{af} = 86\%$. Comparing σ_H and σ_V values (Table 1), we note that our tuned model performs slightly better than the Raizer and Sharkov model.

For a thick layer (Fig. 12b), the experimental e_f values are quite high yet their polarization difference is still visible. To produce such a result, we started tuning our model with $v_{af} = 95\%$ because at this void fraction the model preserves the polarization of e_f (Fig. 10a and Section 5.1.1). Our model underestimated the experimental data by 5.4% for H pol and 3% for V pol. Interestingly, our model could not obtain the high measured values even with $v_{af} = 99\%$. It is not clear whether the use of soap foam in the experiment played some role in causing the high measured e_f values. However, the fact that soap foam seems drier than natural foam [see photographs in Bordonskiy et al. (1978) and Camps et al. (2005)] suggests that we need to emphasize thicker foam layers in the thickness distribution. We thus shifted the peak of the thickness distribution to larger than 3.53 cm by changing σ from the chosen 0.81 cm to 0.7 cm. With this additional tuning and $v_{af} = 98\%$, we simulated the experimental data with quite good agreement of rmse < 1% for both H and V polarizations (Table 1).

5.2.3. Camps et al. (2005) experimental data

Camps et al. (2005) performed emissivity measurements at 1.4 GHz (L-band) of foam created with diffuser in a pool (their Fig. 11). A mix of river water and seawater in different contents provided salinity from 0 to 37 psu; SST ranged from 14 °C to 20 °C. Foam layer thicknesses ranged from about 0.9 cm to 1.7 cm. We use the experimental data of Camps et al. for $t = 1.7$ cm, SST = 18.7 °C and $S = 33.21$ psu (their Fig. 11g) for the comparisons here (Fig. 13).

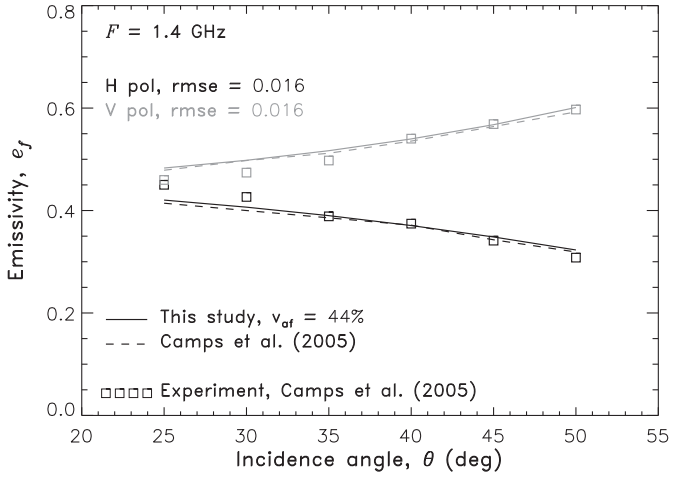

Fig. 13. As Fig. 11 but for experimental and model data of Camps et al. (2005) at a frequency of 1.4 GHz. Stogryn (1972) model is not shown because it is not applicable for this frequency. Details are provided in Section 5.2.3.

Camps et al. (2005) developed a physical foam emissivity model on the basis of the model described by Dombrovskiy and Raizer (1992). The Dombrovskiy and Raizer model is an extension of the Raizer and Sharkov (1982) model aiming to include spray to the seawater–foam system. In contrast to the Raizer and Sharkov model, the foam layer in the Dombrovskiy and Raizer model is not vertically stratified. Camps et al. used a suite of microscopic foam characteristics measured during their experiment as inputs to the model. Their model is optimized by finding the optimal value of one of the bubble parameters which minimizes the rms errors between their measurements and model values [see Table 1 in Camps et al. (2005)]. With this optimization, the Camps et al. model performs quite well, with rms errors ranging from 0.8% to 1.7%. Fig. 13 demonstrates this for the case we use here.

Similar to the previous comparisons, we ran our emissivity model with all elements the same and tuned it by changing only the upper limit of the f_a profile. When tuned to $v_{af} = 44\%$, our model works as well as the Camps et al. model and reproduces the experimental data with an rms error of 1.6% for both H and V polarizations (Table 1). We can make similar comparisons for all cases reported by Camps et al. (2005) and each time we can minimize the rmse between the observations and the model by tuning the v_{af} value. This tuning is equivalent to the Camps et al. (2005) optimization of a bubble parameter mentioned above.

5.3. Evaluation of the foam emissivity model

The experimental data sets used for the comparisons in Section 5.2 cover a frequency range relevant to most current and upcoming satellite radiometers (1 GHz to 37 GHz), a wide range of salinity (0 to 33 psu) and a range of water temperatures (19 °C to 27 °C). With all justified model elements in place and the chosen model inputs, only simple tuning with a single model parameter (the upper limit of the void fraction profile) is needed for our model to reproduce the experimental data with good accuracy, an rms error less than 2% (Table 1).

All physical models to which we compare our model feature a rigorous, explicit account of scattering by densely packed bubbles and involve a suite of microscopic foam characteristics. One of these models is for vertically stratified foam layers (Raizer and Sharkov, 1982); the others are for uniform foam layers (Camps et al., 2005; Chen et al., 2003). The comparisons show that with fewer model variables and inputs, and with a single tuning parameter, our model performs as well as, or better than, the other physical models.

The good agreement between the model and data in Section 5.2 is the result of tuning the upper limit of the void fraction profile v_{af}, either alone or together with a parameter in the thickness distribution. This is in accord with the conclusions of our sensitivity analysis (Section 5.1). The tuned values in Figs. 11 and 12 are within the range of values used in the sensitivity analysis. We can thus put that analysis in the context of the empirical comparisons to judge how robust the good fits from Section 5.2 are. For this purpose, we computed percent difference $\Delta e_{fP\mathrm{exp}} = 100 \cdot |e_{fP\mathrm{mod}} - e_{fP\mathrm{exp}}| / e_{fP\mathrm{exp}}$ where P is polarization (H or V), $e_{f\mathrm{exp}}$ is the emissivity obtained with the experimental values, and $e_{f\mathrm{mod}}$ is the emissivity obtained with the model using either the tuned values or the initially chosen values (Section 4). We found that $\Delta e_{fP\ \mathrm{exp}} \cong \sigma_P$. On this basis, using the results in Fig. 10, we can infer that variability of up to 20% in experimental observations can be predicted by our model with its initial choices with rms error up to 20%. The model tuning that has been used in Fig. 13 is to accommodate much wider variability, and in such cases the model with its currently chosen initial inputs will not perform as well.

This evaluation helps to determine further improvements of the model and thus assist decisions on where to invest research efforts. First and foremost, the range of the void fraction profile should not remain fixed. It will be necessary to account for a varying range of void fractions in foam layers with various thicknesses by using a distribution of the upper limit values; the lower value is not of much significance

and could stay fixed at 1%. The caveat in pursuing this improvement is the lack of any field observations and sufficient laboratory data on the void fraction profile in foam layers. The availability of data, in turn, depends on new experimental developments. A viable alternative meanwhile is analytical consideration of physically justified distributions of the upper limit values; the use of Gaussian distribution is a reasonable starting point.

Another improvement is obtaining and using more data to support or refine the distribution of foam layer thicknesses. It is also necessary to identify the best way to account for the variability of foam emissivity. Though generally correct, the approach of Dombrovskiy and Raizer (1992) still does not account for all possible variations of e_f because both the range of considered thicknesses and the parameters of $p(t)$ are fixed, chosen values, as shown in Section 3.4. The next step of generalization would be to represent the parameters of $p(t)$ as functions of environmental variables, i.e., $e_f[t(U)]$. Then we can use $T_{Bf}(U,t) = W(U).T_s.e_f[t(U)] = W(U).T_s.\int_{t'} e_f(t').p(t')\ dt'$ as a model in which $W(U)$ takes care of the horizontal variability of whitecaps (whitecap fraction) while $e_f[t(U)]$ will take care of the vertical variability (foam layer thickness).

Overall, we consider our foam emissivity model to be as good as possible with the currently available data for sea foam layers. It can be applied successfully to regional cases which would have smaller variability, but should be tuned accordingly when applied to regions with larger variability. With this caution, we surmise that the model can be used for remote sensing of whitecap fraction.

6. Conclusions

Reviewing mechanical, dielectric, and radiative properties of sea foam, we establish requirements for modeling foam emissivity e_f at microwave frequencies (Section 2). Following these requirements and adopting reasonable assumptions and simplifications (Section 3.1), we develop a radiative transfer model of the emissivity of a vertically structured (stratified) layer of sea foam at frequencies from 1 GHz to 37 GHz. The model is in terms of macroscopic foam characteristics, void fraction f_a and foam layer thickness t. The main elements of the model (Sections 3.2–3.4) are the void fraction profile $f_a(z)$ in foam layer depth which brings about a non-uniform profile of foam dielectric and radiative properties; implicit modeling of scattering in foam; and distribution of foam layer thicknesses. The model gives the radiative terms contributing to foam emissivity, such as upwelling and downwelling emission within the foam layer, emission of seawater beneath foam, reflection of downwelling atmospheric emission from the air–foam interface, and multiple reflections at foam layer interfaces.

The results presented here were obtained with an exponential $f_a(z)$ profile with upper (air–foam) and lower (foam-water) limits of 99% and 1%, respectively (Fig. 1); foam permittivity obtained with the refractive mixing rule at seawater temperature $T_s = 20$ °C and salinity $S = 34$ psu (Fig. 2); and a log-normal probability density function $p(t)$ over a range of thicknesses from 0.04 cm to 25 cm peaking at $t = 3.53$ cm (Fig. 3). Conclusions based on these results are:

1) Losses in vertically stratified foam layers are high for 37 GHz and decrease for lower frequencies such as 6.8 GHz and 1.4 GHz (Figs. 4 and 5).
2) Vertically structured foam layers continuously change the incidence angle of the radiation propagating within the foam from its initial value at the air–foam interface (e.g., 53°) to close to nadir incidence at the foam–water interface (Fig. 6).
3) The dependence of foam emissivity on foam layer thickness $e_f(t)$ at various frequencies reveals t values at which different regimes of foam emissivity occur such as the minimal thickness for which foam emissivity is distinguished from the emissivity of the surrounding seawater, the thickness above which foam emissivity reaches saturation and no emissivity variations are observed, and a range of thicknesses between these two limits for which maximum variations of the foam emissivity are expected (Fig. 7a).
4) Different terms contribute to the total emissivity of foam layers and the relative magnitudes of these contributions change for various foam layer thicknesses (Fig. 7b). The strengths of these contributions characterize the foam layers as radiometrically thin foam for which the emission is from the coupled foam–seawater system, radiometrically nominal foam with emission from the foam layer in its entirety, and radiometrically thick foam whose emission is from only part of the foam layer.
5) The dependence of the foam emissivity on incidence angle $e_f(\theta)$ shows high emission (above 0.9) for θ up to about 78° both for specific foam layer thicknesses (Fig. 8) and for a distribution of thicknesses (Fig. 9). Foam depolarizes the radiation propagating within it, i.e., foam emissivity at H or V polarizations has the same dependence on θ.

Analysis of the model sensitivity to the input parameters listed above (Section 5.1) demonstrates that the foam emissivity model is most affected by the choice of the void fraction value at the air–foam interface. The use of a distribution of foam layer thicknesses in the model diminishes, but does not remove, the influence of the foam layer thickness on e_f values. The variations of e_f caused by all other parameters and variables in the model are significantly lower.

Comparisons of the model results to previous experimental and modeling data (Section 5.2) show that our model performs as well as, or better than, other physics-based, as opposed to empirical (Sections 2.3–2.4), models. In addition, the comparisons confirm quantitatively the expected effectiveness of the upper limit of the f_a profile as a tuning parameter. Overall, in addition to accounting for the natural vertical stratification of sea foam, the merits of the model include that it achieves good performance using (i) fewer model variables and inputs, and (ii) a single tuning parameter. The model can be used for the remote sensing of whitecap fraction.

Acknowledgment

This work was sponsored by the Office of Naval Research, NRL Program element 61153N WU 8967. M.A. wishes to thank Karen St. Germain for the support of this work in its initial stage. We thank two anonymous reviewers for their careful review and constructive suggestions that improved the manuscript.

Appendix A

The analytical expressions for the terms in Eq. (6) are obtained following the presentation of the incoherent approach in Ulaby et al. (1981, Section 4–14.2). Let consider the differential energy emitted by a thin horizontal stratum within the foam layer at depth z with thickness dz:

$$dT_{Blstr}(z) = k_{ef}(z).\sec\theta_f(z).T_f(z)dz. \tag{A.1}$$

Sections 2.1 and 3.2.3 of this paper include the definitions of all variables in Eq. (A.1).

The foam optical depths due to strata above and below the stratum at depth z are:

$$\begin{aligned} \tau_{fU} &\equiv \tau_{f\theta}(0,z) = \int_0^z k_{ef}\left(z'\right)\cdot\sec\theta_f\left(z'\right)\cdot dz' \\ \tau_{fD} &\equiv \tau_{f\theta}(z,d) = \int_z^t k_{ef}\left(z'\right)\cdot\sec\theta_f\left(z'\right)\cdot dz'. \end{aligned} \tag{A.2}$$

Due to differing air–water contents above and below depth z, it is expected (and observed) that τ_{fU} and τ_{fD} are quite different.

As justified in Section 3.1, we consider the physical temperature of foam to be constant in depth and equal to that of seawater: $T_f(z) = const = T_s$. Then the brightness temperature at the air–foam boundary due to the entire foam layer is:

$$\begin{aligned} T_{BlstrU} &= T_s \cdot \int_0^t k_{ef}(z) \cdot \sec\theta_f(z) \cdot e^{-\tau_{fU}}\, dz = e_{fU} T_s \\ T_{BlstrD} &= T_s \cdot \int_0^t k_{ef}(z) \cdot \sec\theta_f(z) \cdot e^{-\tau_{fD}}\, dz = e_{fD} T_s. \end{aligned} \tag{A.3}$$

Analogous considerations over seawater half space with a constant permittivity of seawater, and therefore constant seawater extinction coefficient k_w, seawater refraction angle θ_w, and temperature T_s, lead to:

$$T_{BwstrU} = \int_t^\infty k_w \sec\theta_w T_s \cdot e^{-k_w(z-t)\sec\theta_w} dz = T_s. \tag{A.4}$$

Accounting for multiple reflections, the various contributions to foam emissivity are:

$$\begin{aligned} T_{BlU} &= m_U e_{fU} T_s \\ T_{BlD} &= m_D e_{fD} T_s \\ T_{Bw} &= m_w T_s \end{aligned} \tag{A.5}$$

and, according to Eq. (6), their sum gives the total observed signal of the water–foam system. The analytical forms of coefficients m_U, m_D, and m_w in Eq. (A.5) are (Ulaby et al., 1981):

$$\begin{aligned} m_U &= \frac{1-\Gamma_{af}}{1-\Gamma_{af}\Gamma_{fw}/L_f^2} \\ m_D &= \frac{\Gamma_{fw}}{L_f} m_U \\ m_w &= \frac{1-\Gamma_{fw}}{L_f} m_U \end{aligned} \tag{A.6}$$

where indices *af* and *fw* refer to the air–foam and foam–water boundaries (as in Section 3.2.1). Since we consider the foam boundaries to be flat instead of rough (Section 3.1), $\Gamma_{af} = |r_{af}(\theta,\mathrm{P})|^2$ and $\Gamma_{fw} = |r_{fw}(\theta,\mathrm{P})|^2$ represent the specular reflectivity of air–foam and foam–water boundaries obtained with:

$$\begin{aligned} r_{af}^{\mathrm{V}} &= \frac{\varepsilon_{af}\cos\theta - \sqrt{\varepsilon_{af} - \sin^2\theta}}{\varepsilon_{af}\cos\theta + \sqrt{\varepsilon_{af} - \sin^2\theta}} \\ r_{af}^{\mathrm{H}} &= \frac{\cos\theta - \sqrt{\varepsilon_{af} - \sin^2\theta}}{\cos\theta + \sqrt{\varepsilon_{af} - \sin^2\theta}} \end{aligned} \tag{A.7a}$$

and

$$\begin{aligned} r_{fw}^{\mathrm{V}} &= \frac{\varepsilon\sqrt{\varepsilon_{fw} - \sin^2\theta} - \sqrt{\varepsilon.\varepsilon_{fw} - \sin^2\theta}}{\varepsilon\sqrt{\varepsilon_{fw} - \sin^2\theta} - \sqrt{\varepsilon.\varepsilon_{fw} - \sin^2\theta}} \\ r_{fw}^{\mathrm{H}} &= \frac{\sqrt{\varepsilon_{fw} - \sin^2\theta} - \sqrt{\varepsilon.\varepsilon_{fw} - \sin^2\theta}}{\sqrt{\varepsilon_{fw} - \sin^2\theta} - \sqrt{\varepsilon.\varepsilon_{fw} - \sin^2\theta}}. \end{aligned} \tag{A.7b}$$

The ε_{af} and ε_{fw} values in Eq. (A.7a,b) are calculated using the void fraction value at the respective boundary.

The incoherent emissivity and reflectivity of the foam–water system are:

$$e_{inc} = m_U e_{fU} + m_D e_{fD} + m_w = e_{fu} + e_{fd} + e_{ft} \tag{A.8a}$$

$$\Gamma_{inc} = 1 - e_{inc} = 1 - \left(m_U e_{fU} + m_D e_{fD} + m_w\right). \tag{A.8b}$$

The brightness temperature reflected from the foam is $T_{Br} = \Gamma_{inc} T_{sky}$, where T_{sky} is the downwelling atmospheric brightness temperature.

References

Andreas, E. L. (2010). Spray-mediated enthalpy flux to the atmosphere and salt flux to the ocean in high winds. *Journal of Physical Oceanography*, *40*, 608–619.

Andreas, E. L., Persson, P. O. G., & Hare, J. E. (2008). A bulk turbulent air–sea flux algorithm for high-wind, spray conditions. *Journal of Physical Oceanography*, *38*, 1581–1596.

Anguelova, M.D. (2008). Complex dielectric constant of sea foam at microwave frequencies. *Journal of Geophysical Research*, *113*, C08001. http://dx.doi.org/10.1029/2007JC004212.

Anguelova, M., Bettenhausen, M., & Gaiser, P. (2006). Passive remote sensing of sea foam using physically-based models. *Geosci. Rem. Sens. Sym., 2006. IGARSS 2006. IEEE Inter. Conf. on, July 31 2006–Aug. 4 2006* (pp. 3676–3679). http://dx.doi.org/10.1109/IGARSS.2006.942.

Anguelova, M.D., & Gaiser, P. W. (2011). Skin depth at microwave frequencies of sea foam layers with vertical profile of void fraction. *Journal of Geophysical Research*, *116*, C11002. http://dx.doi.org/10.1029/2011JC007372.

Anguelova, M.D., & Gaiser, P. W. (2012). Dielectric and radiative properties of sea foam at microwave frequencies: Conceptual understanding of foam emissivity. *Remote Sensing*, *4*, 1162–1189. http://dx.doi.org/10.3390/rs4051162.

Anguelova, M.D., & Hwang, P. A. (2012). Whitecap fraction of actively breaking waves: Toward a database applicable for dynamic processes in the upper ocean. *18th Air–Sea Interaction Conference, AMS, 19–13 July, Boston, MA* (http://ams.confex.com/ams/20BLT18AirSea/webprogram/Paper209178.html).

Anguelova, M.D., & Webster, F. (2006). Whitecap coverage from satellite measurements: A first step toward modeling the variability of oceanic whitecaps. *Journal of Geophysical Research*, *111*, C03017. http://dx.doi.org/10.1029/2005JC003158.

Barber, R. P., Jr., & Wu, J. (1997). Sea brightness temperature and effects of spray and whitecaps. *Journal of Geophysical Research*, *102*(C3), 5823–5827. http://dx.doi.org/10.1029/96JC03760.

Bettenhausen, M. H., Smith, C. K., Bevilacqua, R. M., Wang, N. -Y., Gaiser, P. W., & Cox, S. (2006). A nonlinear optimization algorithm for WindSat wind vector retrievals. *IEEE Transactions on Geoscience and Remote Sensing*, *44*, 597–610.

Blanchard, D. C. (1963). The electrification of the atmosphere by particles from bubbles in the sea. *Progress in Oceanography*, *1*, 71–202.

Bordonskiy, G. S., Vasilkova, I. B., Veselov, V. M., Vorsin, N. N., Militskiy, Yu. A., Mirovskiy, V. G., et al. (1978). Spectral characteristics of the emissivity of foam formations. *Izvestiya, Atmospheric and Oceanic Physics*, *14*, 464–469.

Brekhovskikh, L. M. (1980). Reflection reduction of optical systems. *Waves in layered media* (pp. 1–224). New York: Academic Press.

Camps, A., Vall-llossera, M., Villarino, R., Reul, N., Chapron, B., Corbella, I., et al. (2005). The emissivity of foam-covered water surface at L-band: Theoretical modeling and experimental results from the FROG 2003 field experiment. *IEEE Transactions on Geoscience and Remote Sensing*, *43*, 925–937.

Chen, D., Tsang, L., Zhou, L., Reising, S.C., Asher, W. E., Rose, L. A., et al. (2003). Microwave emission and scattering of foam based on Monte Carlo simulations of dense media. *IEEE Transactions on Geoscience and Remote Sensing*, *41*, 782–790.

de Leeuw, G., Andreas, E. L., Anguelova, M.D., Fairall, C. W., Lewis, E. R., O'Dowd, C., et al. (2011). Production flux of sea spray aerosol. *Reviews of Geophysics*, *49*, RG2001. http://dx.doi.org/10.1029/2010RG000349.

Deane, G. B., & Stokes, M.D. (2002). Scale dependence of bubble creation mechanisms in breaking waves. *Nature*, *418*, 839–844.

Dombrovskiy, L. A. (1979). Calculation of thermal radio emission from foam on the sea surface. *Izvestiya, Atmospheric and Oceanic Physics*, *15*, 193–198.

Dombrovskiy, L. A., & Raizer, V. Y. (1992). A microwave model of 2-phase medium near the ocean surface. *Izvestiya Akademii Nauk Fizika Atmosfery I Okeana*, *28*, 863–872.

Droppleman, J. (1970). Apparent microwave emissivity of sea foam. *Journal of Geophysical Research*, *75*, 696–698.

Gaiser, P. W., St Germain, K. M., Twarog, E. M., Poe, G. A., Purdy, W., Richardson, D., et al. (2004). The WindSat spaceborne polarimetric microwave radiometer: Sensor description and early orbit performance. *IEEE Transactions on Geoscience and Remote Sensing*, *42*, 2347–2361.

Guo, J., Tsang, L., Asher, W., Ding, K. -H., & Chen, C. -T. (2001). Applications of dense media radiative transfer theory for passive microwave remote sensing of foam covered ocean. *IEEE Transactions on Geoscience and Remote Sensing*, *39*, 1019–1027.

Ishimaru, A., & Kuga, Y. (1982). Attenuation constant of a coherent field in a dense distribution of particles. *Journal of the Optical Society of America*, *72*, 1317–1320.

Jessup, A. T., Zappa, C. J., Loewen, M. R., & Hesany, V. (1997). Infrared remote sensing of breaking waves. *Nature*, *385*, 52–55.

Klein, L. A., & Swift, C. T. (1977). An improved model for the dielectric constant of sea water at microwave frequencies. *IEEE Transactions on Antennas and Propagation*, *AP-25*, 104–111.

Koepke, P. (1986). Remote sensing signatures of whitecaps. In E. C. Monahan, & G. M. Niocaill (Eds.), *Oceanic whitecaps* (pp. 251–260). Dordrecht: Reidel.

Kokhanovsky, A. (2004). Spectral reflectance of whitecaps. *Journal of Geophysical Research*, *109*, C05021. http://dx.doi.org/10.1029/2003JC002177.

Landau, L. D., & Lifshitz, E. M. (1960). *Electrodynamics of continuous media*. Reading, Massachusetts, USA: Addison-Wesley, 293–309.

Leifer, I., & de Leeuw, G. (2006). Bubbles generated from wind-steepened breaking waves: 1. Bubble plume bubbles. *Journal of Geophysical Research*, *111*, C06020. http://dx.doi.org/10.1029/2004JC002673.

Lewis, E. R., & Schwartz, S. E. (2004). *Sea salt aerosol production: Mechanisms, methods, measurements and models : A critical review*. Washington, DC: American Geophysical Union, 413.

Meissner, T., & Wentz, F. (2002). An updated analysis of the ocean surface wind direction signal in passive microwave brightness temperatures. *IEEE Transactions on Geoscience and Remote Sensing*, *40*, 1230–1240.

Militskii, Y. A., Raizer, V. Y., Sharkov, E. A., & Etkin, V. S. (1978). Thermal radio emission from foam structures. *Soviet Physics—Technical Physics*, *23*, 601–602.

Monahan, E. C., Fairall, C. W., Davidson, K. L., & Boyle, P. J. (1983). Observed inter-relations between 10 m winds, ocean whitecaps and marine aerosols. *Quarterly Journal of the Royal Meteorological Society*, *109*, 379–392.

Newell, A.C., & Zakharov, V. E. (1992). Rough sea foam. *Physical Review Letters*, *69*, 1149–1151.

Nordberg, W., Conaway, J., Ross, D. B., & Wilheit, T. (1971). Measurements of microwave emission from a foam-covered, wind-driven sea. *Journal of Atmospheric Sciences*, *28*, 429–435.

Odelevskiy, V. I. (1951). Calculation of generalized conductance of heterogeneous systems 1. Matrix two phase systems with nonelongated inclusions. *Zhurnal Tekhnicheskoi Fiziki*, *21*, 667–685.

Padmanabhan, S., Reising, S.C., Asher, W. E., Rose, L. A., & Gaiser, P. W. (2006). Effects of foam on ocean surface microwave emission inferred from radiometric observations of reproducible breaking waves. *IEEE Transactions on Geoscience and Remote Sensing*, *44*, 569–583.

Peake, W. (1959). Interaction of electromagnetic waves with some natural surfaces. *IRE Transactions on Antennas and Propagation*, *7*(Spec. Suppl.), S324–S329.

Peltzer, R. D., & Griffin, O. M. (1987). The stability and decay of foam in sea water. *Ocean physics and engineering*, *12*, 101–126.

Plant, W. J. (2003). Microwave sea return at moderate to high incidence angles. *Waves in Random Media*, *13*, 339–354.

Raizer, V. (2007). Macroscopic foam-spray models for ocean microwave radiometry. *IEEE Transactions on Geoscience and Remote Sensing*, *45*, 3138–3144.

Raizer, V. Ya, & Sharkov, E. A. (1982). Electrodynamic description of densely packed dispersed systems. *Izvestiya Radiophys and Quantum Electronics*, *24*, 553–560.

Reising, S.C., Asher, W. E., & Rose, L. A. (2002). Polarimetric emissivity of whitecaps experiment (POEWEX): Preliminary results. *WindSat Science Workshop, November*. Arlington, VA: Noesis, Inc.

Reul, N., & Chapron, B. (2003). A model of sea–foam thickness distribution for passive microwave remote sensing applications. *Journal of Geophysical Research*, *108*(C10), 3321. http://dx.doi.org/10.1029/2003JC001887.

Rose, L. A., Asher, W. E., Reising, S.C., Gaiser, P. W., St Germain, K. M., Dowgiallo, D. J., et al. (2002). Radiometric measurements of the microwave emissivity of foam. *IEEE Transactions on Geoscience and Remote Sensing*, *40*, 2619–2625.

Rosenkranz, P. W., & Staelin, D. H. (1972). Microwave emissivity of ocean foam and its effect on nadiral radiometric measurements. *Journal of Geophysical Research*, *77*, 6528–6538.

Sharkov, E. A. (2003). *Passive microwave remote sensing of the earth*. Chichester, UK: Praxis.

Sihvola, A. (1999). *Electromagnetic mixing formulas and applications*. London: The Institute of Electrical Engineers, London.

Smith, P.M. (1988). The emissivity of sea foam at 19-Ghz and 37-Ghz. *IEEE Transactions on Geoscience and Remote Sensing*, *26*, 541–547.

Stogryn, A. (1970). Brightness temperature of a vertically structured medium. *Radio Science*, *5*, 1397–1406.

Stogryn, A. (1972). The emissivity of sea foam at microwave frequencies. *Journal of Geophysical Research*, *77*, 1658–1666.

Stogryn, A. P. (1997). *Equations for the permittivity of sea water*. Report to the Naval Research Laboratory, Washington, DC, USA.

Tang, C. C. H. (1974). The effect of droplets in the air–sea transition zone on the sea brightness temperature. *Journal of Physical Oceanography*, *4*, 579–593.

Troitsky, V. (1962). Radio emission of the moon, its physical state, and the nature of its surface. In Z. Kopal, & Z. Mikhailov (Eds.), *The Moon* (pp. 475–489). New York: Elsevier.

Tsang, L. (1992). Dense media radiative transfer theory for dense discrete random media with particles of multiple sizes and permittivities. *Progress in Electromagnetics Research*, *6*, 181–230.

Tsang, L., Chen, C. -T., Chang, A. T. C., Guo, J., & Ding, K. -H. (2000). Dense media radiative transfer theory based on quasicrystalline approximation with applications to passive microwave remote sensing of snow. *Rad. Sci.*, *35*, 731–749.

Tsang, L., Kong, J. A., & Shin, R. T. (1985). *Theory of microwave remote sensing*. New York: Wiley&Sons.

Tsang, L., Mandt, C. E., & Ding, K. H. (1992). Monte Carlo simulations of the extinction rate of dense media with randomly distributed dielectric spheres based on solution of Maxwell's equations. *Optics Letters*, *17*, 314–316.

Tsang, L., Njoku, E., & Kong, J. A. (1975). Microwave thermal emission from a stratified medium with nonuniform temperature distribution. *Journal of Applied Physics*, *46*, 5127–5133. http://dx.doi.org/10.1063/1.321571.

Ulaby, F., Moore, R., & Fung, A. (1981). *Microwave remote sensing: Active and passive, Vol. I*, Reading, Massachusetts, USA: Addison-Wesley Publishing Company.

Ulaby, F., Moore, R., & Fung, A. (1982). *Microwave remote sensing: Active and passive: Radar remote sensing and surface scattering and emission theory, Vol. II*, Reading, Massachusetts, USA: Addison-Wesley Publishing Company.

Ulaby, F., Moore, R., & Fung, A. (1986). *Microwave remote sensing: Active and passive, Vol. III*, Dedham, Massachusetts, USA: Artech House, Inc.

Wanninkhof, R., Asher, W., Ho, D., Sweeney, C., & McGillis, W. (2009). Advances in quantifying air–sea gas exchange and environmental forcing. *Annual Review of Marine Science*, *1*, 213–244.

Wentz, F. J. (1974). *The effect of surface roughness on microwave sea brightness temperatures*. Final Report. Wakefield, Massachusetts, USA: Radiometric Technology, Inc.

Wentz, F., & Meissner, T. (2000). *Algorithm theoretical basis document (atbd): Amsr ocean algorithm*. RSS Tech. Proposal 121599A-1. Santa Rosa, California, USA: Remore Sensing Systems.

Wilheit, T. T. (1978). Radiative-transfer in a plane stratified dielectric. *IEEE Transactions on Geoscience and Remote Sensing*, *16*, 138–143.

Wilheit, T. T. (1979). Effect of wind on the microwave emission from the ocean's surface at 37-GHz. *Journal of Geophysical Research*, *84*, 4921–4926.

Williams, G. F. (1971). Microwave emissivity measurements of bubbles and foam. *IEEE Transactions on Geoscience Electronics, GE-9*, 221–224.

Zhang, Y., Yang, Y. E., & Kong, J. A. (2002). A composite model for estimation of polarimetric thermal emission from foam-covered wind-driven ocean surface. *Progress in Electromagnetics Research*, *37*, 143–190. http://dx.doi.org/10.2528/PIER02040800.

Zhou, L., Tsang, L., & Chen, D. (2003). Polarimetric passive microwave remote sensing of wind vectors with foam-covered rough ocean surfaces. *Radio Science*, *38*, 1073. http://dx.doi.org/10.1029/2002RS002764.

Zine, S., Boutin, J., Font, J., Reul, N., Waldteufel, P., Gabarro, C., et al. (2008). Overview of the SMOS sea surface salinity prototype processor. *IEEE Transactions on Geoscience and Remote Sensing*, *46*, 621–645. http://dx.doi.org/10.1109/TGRS.2008.915543.

Zurk, L. M., Tsang, L., Ding, K. H., & Winebrenner, D. P. (1995). Monte Carlo simulations of the extinction rate of densely packed spheres with clustered and nonclustered geometries. *Journal of the Optical Society of America. A*, *12*, 1772–1781.